The TRIP Effect and Its Application in Cold Formable Sheet Steels

Wolfgang Bleck,* Xiaofei Guo, and Yan Ma

The Transformation-Induced-Plasticity (TRIP) effect is used for enhancing the formability of cold formable sheet steels. While the first observation of this phenomenon dates back to the 1930's, the industrial usage of the TRIP steels started after 1950. First fully austenitic steels, later on multiphase steels have been developed with a meta-stable austenitic phase that can transform stress-assisted or strain-induced into ε- or α'-martensite during deformation. The historic development, the principles of the TRIP effect, and the different groups of steels using the TRIP effect are described. For the already commercialized TRIP steels, characteristic chemical compositions and microstructures are discussed; the requirements for the process design as well as new annealing concepts after cold rolling are explained.

1. Definition of the TRIP Effect

The Transformation-Induced-Plasticity (TRIP) effect in steels denotes the significant enhancement of both strength and ductility through austenite to martensite transformation during the plastic deformation.[1] The transformation of (retained) austenite to martensite during deformation at or close to room temperature develops a high carbon martensite phase, which substantially raises the strain-hardening rate and strengthens the material effectively, as shown in **Figure 1**.[2] The progressive transformation of austenite to martensite during straining is visible in the serrations and leads to high strain hardening and postponed occurring of necking. Accordingly, the material's ductility retains or increases in spite of higher strength.

2. Steels with TRIP Effect

In the 1930's, Scheil[3,4] observed the formation of martensite needles in Fe–Ni alloys, which underwent shear forces. He raised two hypotheses: one is the stress hypothesis that the martensite transformation needs a minimum shear stress; another is the instability hypothesis that the transformation occurs spontaneously when the martensitic transformation temperature is reached unless a reverse stress is applied. Wassermann[5,6] also observed the orientation dependent martensitic transformation in Fe–Ni alloys under tensile deformation. The transformation contributes to the material ductility.[6,7] In the following decades, the study on the austenite to martensite transformation behaviors in Fe–Ni alloys was conducted in many different aspects, including the thermodynamics,[8–11] the factors influencing the phase transformation, such as temperature,[12–14] stress, and strain paths.[15,16]

The first proposal for the practical exploitation of TRIP steels came from Zackay and his co-workers.[1] They defined high-alloyed austenitic steels with nickel and other austenite stabilizing elements as TRIP steels, which are termed as Meta-stable Austenitic Stainless Steels (Meta-stable ASS) nowadays. By quenching the high-alloyed austenitic steels in liquid nitrogen after hot rolling, a significant amount of retained "meta-stable" austenite is produced. These alloys obtained significantly improved uniform elongation up to ≈80% through deformation-induced martensitic transformation.[17] The meta-stable austenitic phase at ambient temperature is achieved by large concentrations of Ni and other expensive austenite stabilizing elements. Fahr et al. further defined the "stress-induced" and "strain-induced" formation of martensite and found that a specific amount of strain-induced martensite led to an "optimum" work hardening rate and resulted in high strength and high ductility in meta-stable ASS.[18] The good combination of mechanical properties and the intended reduction in high-cost alloying elements led to many research activities and industrialization of meta-stable ASS.

In the 1980's, the TRIP effect was demonstrated by Matsumura et al.[19,20] in low-alloy steels consisting of 0.2–0.4 wt%C, 1–2 wt%Mn, and 1–2 wt%Si. These alloys consists of 40–60 vol% allotriomorphic ferrite, 35–45 vol% carbide-free bainite, and the remainder being high-carbon

[*] Prof. Dr. W. Bleck, Dr. X. Guo, Y. Ma
Steel Institute, RWTH Aachen University, Intzestraße 1, 52072 Aachen, Germany
Email: bleck@iehk.rwth-aachen.de

DOI: 10.1002/srin.201700218

retained austenite with or without martensite. Distinguished from the meta-stable ASS with a fully austenitic microstructure prior to deformation, these steels are termed as TRIP-assisted low alloy steels or low-carbon TRIP steels. The low-carbon TRIP steels typically contain 5–15 vol% retained austenite.[21–24] They belong to the group termed first-generation Advanced High Strength Steels (AHSS). The first-generation AHSS consist of multiphase high strength cold formable steels with a ferritic matrix and improved formability compared with conventional high strength steels. In comparison to the other first-generation AHSS with equivalent strength, such as dual-phase (DP) steels, the TRIP steels offer improved ductility and strain-hardening capability.[25,26] The ECO Index (ECO Index = ultimate tensile strength × uniform elongation) of low-carbon TRIP is usually approaching 20 000 MPa%.[27]

Prof. Dr. Wolfgang Bleck is head of the Steel Institute of RWTH Aachen University. He obtained his Dr. degree at TU Clausthal in 1979, worked in a steel company from 1980 till 1993, and then became professor at RWTH Aachen University. He is speaker of the Collaborative Research Centre SFB 761 "Steel-*ab initio*: quantum mechanics guided design of new Fe based materials".

Dr. Xiaofei Guo is scientific researcher in the steel institute, RWTH Aachen University. She obtained her Ph.D degree in Steel Institute, RWTH Aachen University in 2012 on the topic of "Influences of Microstructure, Alloying Elements and Forming Parameters on Delayed Fracture in TRIP/TWIP-Aided Austenitic Steels". She works on projects concerning the deformation and fracture mechanisms in TRIP-assisted steels.

Yan Ma, M.Sc. obtained his bachelor degree in 2013 from University of Science and Technology Beijing, China, and master degree in 2015 from RWTH Aachen University, Germany. Since 2016, he has been working in the Steel Institute of RWTH Aachen University as a scientific researcher. His research topic focuses on the microstructure - mechanical properties relationship of high-Mn and medium-Mn steels.

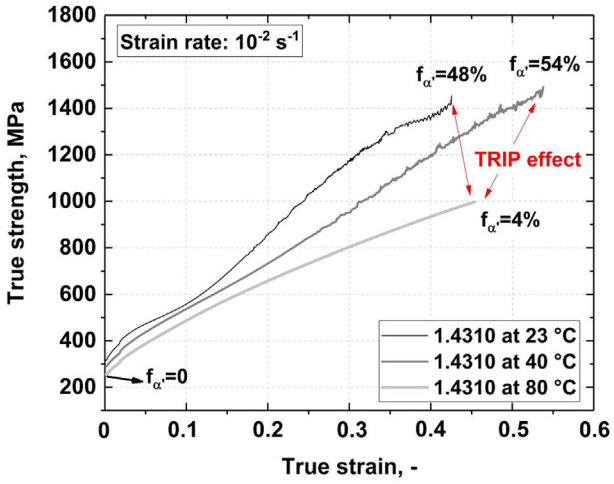

Figure 1. Flow curves of a meta-stable austenitic stainless grade 1.4310. (DIN EN 10088) The strain induced α' martensite formation has been measured using a FISCHER ferritscope considering a calibration factor of 1.7.[2]

Based on the research on Hadfields steel, in 1962, White et al.[28] observed the TRIP effect in Fe–Mn–C high-manganese steels by adjustment of the chemical composition. In 1986, Tomota et al.[29] reported the TRIP effect in the Fe–Mn binary alloys with various Mn contents (16–36 wt%). Both the $\gamma \rightarrow \varepsilon$ and the $\varepsilon \rightarrow \alpha'$ transformation were observed during deformation. It was documented that the $\gamma \rightarrow \varepsilon$ transformation could effectively improve the strain-hardening rate in high-manganese steels by composition optimization. Since the 2000s, high-manganese steels have been intensively studied owing to their excellent balance of high strength and superior ductility.[30,31] The ECO Index of high-manganese steels lies in the range of 50 000 to 60 000 MPa%. This innovative steel group with a fully austenitic matrix is termed as second-generation AHSS.

In 2003, Speer et al.[32] first proposed a novel process – Quenching and Partitioning (Q&P) – to develop a martensitic steel with a certain amount of retained austenite. The austenite phase is stabilized by carbon partitioning between martensite and untransformed austenite, processing via an isothermal heat treatment after quenching to a temperature between martensite transformation start temperature (M_s) and martensite transformation finish temperature (M_f). The deformation-induced transformation of retained austenite contributes to the high strain-hardening rate and improves the ductility of martensitic steels. Since the 2010s, the medium-manganese steels have attracted intensive interest of materials scientists.[33–35] Previously, the TRIP effect in medium-manganese steels was first reported by Miller[36] in 1972. The Fe–5.7Mn–0.11C (wt%) steel was intercritically annealed in the $\gamma + \alpha$ region, resulting in ultrafine grained (UFG) duplex microstructure with 10–30 vol% austenite.[36] This UFG medium-manganese steel revealed high ultimate tensile strength (UTS) of

1145 MPa and 30.5% total elongation (TEL).[36] The specific heat treatment in the intercritical region used to process the medium-manganese steels with UFG microstructure is termed as Austenite-Reverted-Transformation (ART) annealing. The mechanical properties of Q&P steels and medium-manganese steels fill the gap between the first-generation AHSS and the second-generation AHSS. They are referred to as the third-generation AHSS. The ECO index of the third-generation AHSS is about 30 000–4 000 MPa%.

In 2009, the TRIP effect was further explored in maraging steels. Raabe et al.[37] proposed a new concept to enhance the strength and ductility simultaneously by the combination of TRIP effect and martensite aging (Maraging) effect. Benefiting from both the occurrence of the TRIP effect during deformation and nano-sized intermetallic precipitation strengthening by aging, this steel grade develops a high UTS up to 1.5 GPa and total elongations between 15 and 20%.[37,38] During the aging of martensite, a pronounced austenite reversion takes place as well and the elemental partitioning of C and a small amount of Mn at the martensite/austenite interface results in the formation and growth of a new austenite layer.[39] The deformation-induced transformation from reversed austenite to α'-martensite during deformation leads to an improved ductility.

More recently, Li et al.[40] reported a new class of TRIP assisted high-entropy dual-phase alloys. By appropriate adjustment of chemical composition in high entropy alloys (HEAs), the meta-stable dual-phase microstructure is achieved in Fe50Mn30Co10Cr10 TRIP-DP-HEAs.[40] The microstructure of the HEA prior to deformation consists of about 72% face-centered cubic (f.c.c.) phase and 28% hexagonal close-packed (h.c.p.) phase. Up to post-necking stage, approximately 56% f.c.c. phase transforms into h.c.p. phase.[40] As a result, this material achieves the tensile strength of over 850 MPa and total elongation of ≈75%, which overcomes the strength-ductility paradoxon in conventional high strength steels. It is believed that the newly generated phase boundaries owing to deformation-induced transformation acts as additional obstacles of dislocation slip, thereby enhancing the strain hardening.[40]

In summary, the steels utilizing TRIP effect cover a wide range of steels. The presence of meta-stable austenite phase at room temperature is realized through high alloying or element enrichment. The chronological development of different steels with TRIP-effect is summarized in **Figure 2**. The typical chemical compositions and microstructures are listed in **Table 1**. The typical mechanical properties represented by the ultimate tensile strength (UTS) and total elongation (TEL) values are described in **Figure 3**.

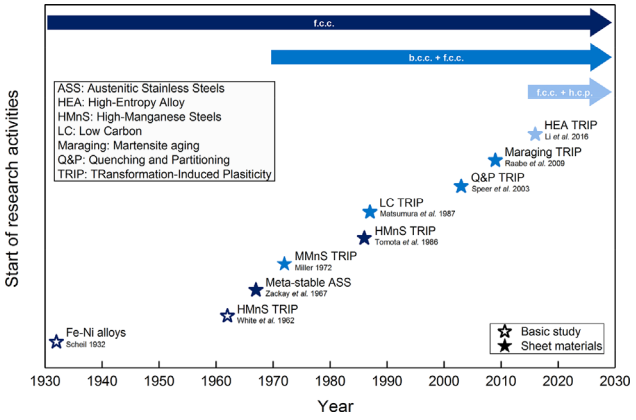

Figure 2. Chronological development of research work on steels utilizing TRIP effect.

3. Martensitic Transformation Mechanisms

Austenite to martensite transformation follows the displacive mechanism, which is a diffusionless shear transformation. The deformation takes place on habit planes and follows preferred directions.[59] The transformation from f.c.c. to body-centered cubic (b.c.c.) crystal structure occurs with 24 possible variants with distinct lattice orientation relationship, within which only the preferred variants are nucleated upon thermomechanical loading depending on the stress and stress state.[8,60,61] Entrapped carbon raises the tetragonality of the b.c.c. structure, therefore, martensite in steels is a body-centered tetragonal (b.c.t.) phase. The crystallography of martensite transformation has been reviewed by Kelly.[62]

There are three types of martensitic transformation according to the driving force: (i) Athermal martensitic transformation; (ii) Stress-assisted martensitic transformation, and (iii) Strain-induced martensitic transformation. Athermal martensitic transformation is a thermodynamically driven process, which is only temperature dependent. M_s is used to denote the start temperature for martensitic transformation. The stress-assisted martensitic transformation occurs at the temperature above M_s with the presence of mechanical driven force U. Patel and Cohen[8] interpreted the mechanical driving force U as dependent on the applied shear stress τ and normal stress σ, where γ_0 and ε_0 are the transformation shear and dilatation strains, respectively, as shown in Equation 1. The mechanical driven force has linear dependencies on the applied stresses, as well as being greatly affected by the stress states.

$$U = \tau\gamma_0 + \sigma\varepsilon_0 \tag{1}$$

Fahr et al.[18] put forward that the austenite to martensite transformation is driven by both stress and strain. Olson and Cohen[63] generalized this behavior and produced the schematic diagram based on the experimental results of Bolling and Richman[64] to describe the influences of stress and strain on martensitic transformation temperature, which are shown in **Figure 4**. When the material is cooled from the austenitic region to the temperature below M_s, the transformation starts athermally. As discussed above, when the mechanical

Steel designation	Typical chemical composition, wt% (Fe balanced)									Special process	Microstructure
	C	Si	Mn	Cr	Mo	Ni	Al	Co	Ti		
Meta-stable ASS	0.02–0.15	n/a	0–6	17–20	n/a	3–7	n/a	n/a	n/a	no	γ(100%)
LC TRIP	0.1–0.3	1–2	1–2	n/a	n/a	n/a	1–2	n/a	n/a	Intercritical annealing	α(40–60%) $+\alpha_B$(35–45%) $+\gamma_R$(5–15%)
HMnS TRIP	0.1–0.6	0–3	14–23	n/a	n/a	n/a	0–3	n/a	n/a	no	γ(100%)
Q&P TRIP	0.1–0.3	1–2	1.5–3	n/a	n/a	n/a	n/a	n/a	n/a	Q&P treatment	$\alpha' + \gamma$(5–10%) + (α)
MMnS TRIP	0.05–0.4	0–3	4–12	n/a	n/a	n/a	0–2	n/a	n/a	ART annealing	$\alpha + \gamma$(20–40%)
Maraging TRIP	0.01	0.06	12	n/a	1	2	0.1	n/a	1	Aging treatment	$\alpha' + \gamma(\approx 15\%)$
HEA TRIP	0–0.5	n/a	30–45	10	n/a	n/a	n/a	10	n/a	no	$\varepsilon + \gamma(\approx 30\%)$

ASS: Austenitic Stainless Steels; LC: Low Carbon; TRIP: Transformation-Induced Plasticity; HMnS: High-Manganese Steels; MMnS: Medium-Manganese Steels; Q&P: Quenching and Partitioning; Maraging: Martensite Aging; HEA: High Entropy Alloy; ART: Austenite Reverted Transformation.

Table 1. Chemical composition and microstructure of steels utilizing TRIP effect.

driving force exists, the M_s temperature rises linearly with the applied stress till the yield stress of austenite, as shown in Part I in Figure 4. When the stress required for transformation exceeds the yield strength of the material, plastic strain precedes transformation, as illustrated in Figure 4 Part II. Olson and Cohen[65] assumed the plastic strain produces shear band intersections, which act as nucleation sites for martensitic transformation. As a result, the required stress is lower than the pure stress condition. When the maximum temperature limit M_d is reached, the austenite can only deform plastically, as shown in Figure 4 Part III. In this condition, the chemical driving force is too small to nucleate martensite even with the external mechanical loading.

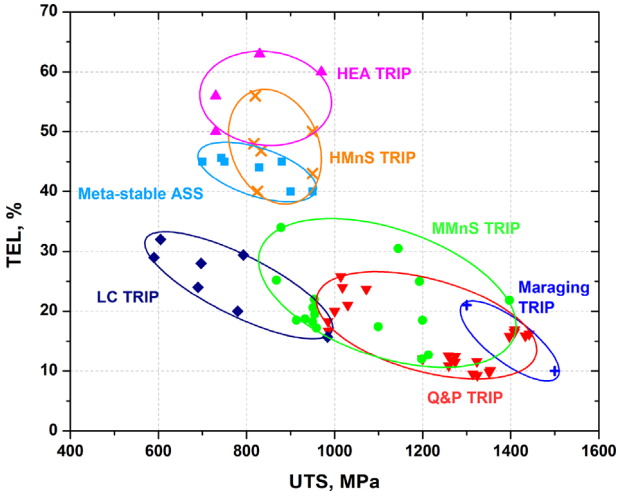

Figure 3. The total elongation (TEL) versus ultimate tensile strength (UTS) diagram for steels utilizing the TRIP effect; representative mechanical properties of HMnS TRIP,[41–43] Q&P TRIP,[44–49] MMnS TRIP,[36,50–54] Maraging TRIP,[37] HEA TRIP[55,56] from literature, LC TRIP from Autosteel website,[57] and Meta-stable ASS from standard EN10088-2.[58]

Lo et al.[66] reviewed the potential nucleation sites and transformation routines of deformation induced martensite. The energetically favorable nucleation sites are the intersections of shear bands,[67] inside shear bands,[67] the intersections of shear bands with grain boundaries,[67] the intersections of ε-martensite,[68] inside single ε-martensite,[69] the intersection of twinning plates,[70] and even dislocation pile-ups[71] etc. Shear bands designate the thin bands with large localized shear strains. They usually cross several grains. The shear bands may contain mechanical twins, ε-martensite, and bundles of stacking faults or slip bands.[65] Depending on the nature of the overlapping, twins, ε-martensite or stacking fault bundles may form. Twins form when stacking faults overlap on successive {111} planes, whereas the ε martensite is generated if the overlapping of stacking faults occurs on alternate {111} planes. Stacking fault bundles arise from the irregular overlapping of stacking faults.[66] In general, the nucleation sites of α'-martensite are associated with various lattice defects existing in the microstructure, where the local stress due to the lattice misfit favors the transformation. Many factors, such as forming condition, grain size, material chemistry, influence the favorable martensite nucleation sites, and transformation paths.[66] The martensitic transformation can proceed through both $\gamma \rightarrow \varepsilon \rightarrow \alpha'$ or $\gamma \rightarrow \alpha'$ routines, which is quite dependent on the deformation temperature.[66,72]

The transformation behavior has also been described by phenomenological or constitutive models. Angel first developed an empirical formula to calculate the volume

of transformed martensite on the degree of plastic deformation.[73] Olson and Cohen proposed a temperature dependent model to describe martensitic transformation kinetics based on the observations of intersections of shear systems.[65] As shown in Equation 2, the volume fraction of martensite $f^{\alpha'}$ obtained at the strain ε is affected by the temperature dependent parameters, α and β. The former depends on the Stacking Fault Energy (SFE) of the steel, which in turn is affected by material chemistry and temperature. β is related to the probability that an intersecting shear system creates a nucleation site and the driving force for $\gamma \rightarrow \alpha'$ transformation. The exponent n is a dimensionless constant, which is used as a fitting parameter. It usually has a value ≥ 2. For examples, a value of 4.5 is appropriate for the steels studied by Angel.[73] The n constant is affected by the material and process parameters, which influence the transformation kinetics.

$$f^{\alpha'} = 1 - \exp[-\beta(1 - \alpha\varepsilon)^n] \quad (2)$$

Much research work was carried out to improve the Olson-Cohen model by incorporating the critical factors, such as stress state,[74–79] strain rate[76,80] etc. The constitutive relation describing the transformation-induced plasticity provides opportunity for effective material and process design of TRIP-assisted steels.

4. TRIP Effect in Meta-Stable Austenitic Stainless Steels

Meta-stable ASS contain reduced Ni alloying compared with the conventional stable ASS. The strain-induced martensitic transformation is initiated at room temperature. Meta-stable ASS usually have a fully austenitic structure in the cold rolled and annealed condition. The unstable austenite transforms progressively to α'- and/or ε-martensite upon the applied plastic deformation. As a result, they achieve extraordinary mechanical properties through transformation strengthening. The typical chemical composition of commercial meta-stable ASS are listed in **Table 2**.[58] The alloying elements of C, N, or Mn are added to partially replace the Ni element for stabilizing the austenite phase at room temperature. The contribution of these elements in stabilizing the austenite phase is empirically described by the Ni equivalent, as listed in **Table 3**.

The stability of the austenite structure is controlled by the SFE, which describes the interaction between the extended dislocations on the closely spaced slip planes.[81,82] When the SFE is low, the mobility of dislocations is greatly suppressed; the dissociation of a full dislocation into two partials is energetically favorable. The stacking sequence changes to the faulted sequence, which involves h.c.p. stacking and provides nuclei for

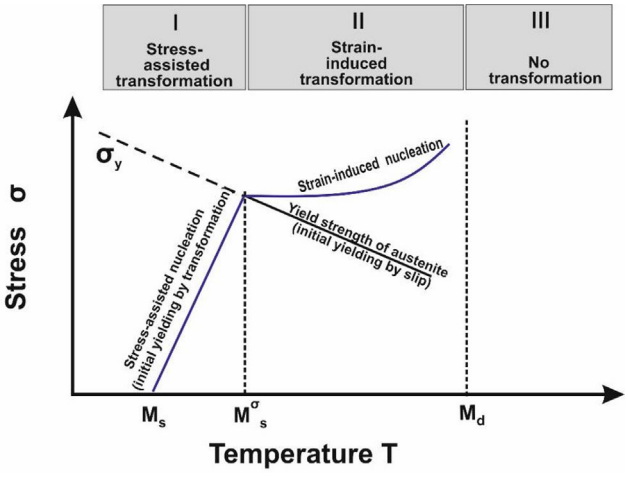

Figure 4. Schematic illustration of the critical stress to initiate martensitic transformation as a function of temperature, according to Olson and Cohen.[63]

		Chemical composition, wt% (max.)					
Steel grade	**Material Number**	**C**	**Cr**	**Ni**	**Mn**	**N**	**Microstructure**
X5CrNi18-10	1.4301	0.07	17.5–19.5	8.0–10.5	2.0	0.11	pure austenite
X2CrNi18-9	1.4307	0.03	17.5–19.5	8.0–10.5	2.0	0.11	pure austenite
X10CrNi18-8	1.4310	0.15	16.0–19.0	6.0–9.5	2.0	0.11	pure austenite
X2CrNiN18-7	1.4318	0.03	16.5–18.5	6.0–8.0	2.0	0.10–0.20	pure austenite
X12CrMnNiN17-7-5	1.4372	0.15	16.0–18.0	3.5–5.5	5.5–7.5	0.05–0.25	pure austenite
X8CrMnNiN19-6-3	1.4376	0.10	17.0–20.5	2.0–4.5	5.0–8.0	0.30	pure austenite

Table 2. Chemical composition and microstructure of some commercial meta-stable austenitic stainless steels according to standard EN 10088-2.[58]

	Formulae	Author	Ref.
Ni_{eq}	$Ni_{eq} = \%\ Ni + 0.65\%Cr + 0.98\%Mo + 1.05\%Mn + 0.35\%Si + 12.6\%C$	Rhodes, et al.	[84]
	$Ni_{eq} = \%Ni + 0.6\%Mn + 0.18\%Cr + 9.69(\%C+\%N) - 0.11(\%Si)^2$	Takemoto, et al.	[85]
SFE	$SFE(mJ/m^2) = -53 + 6.2\%Ni + 0.7\%Cr + 3.2\%Mn + 9.3\%Mo$	Schramm, et al.	[81]
	$SFE(mJ/m^2) = 1.2 + 1.4\%Ni + 0.6\%Cr + 7.7\%Mn - 44.7\%Si$	Rhodes, et al.	[84]
	$SFE(mJ/m^2) = -25.7 + 2\%Ni + 410\%C - 0.9\%Cr - 77\%N - 13\%Si - 1.2\%Mn$	Pickering	[86]
	$SFE\gamma^{300}(mJ/m^2) = \gamma^0 + 1.59\%Ni - 1.34\%Mn + 0.06(\%Mn)^2 - 1.75\%Cr + 0.01(\%Cr)^2 + 15.12\%Mo - 5.59\%Si - 60.69\,(\%C + 1.2\%N)^{(1/2)} + 26.27(\%C + 1.2\%N)(\%Cr+\%Mn+\%Mo)^{(1/2)} + 0.61[\%Ni(\%Cr + \%Mn)]^{(1/2)}$ (γ^{300} is the value of SFE at room temperature; γ^0 is the value of SFE of pure austenitic iron at room temperature)	Dai, et al.	[87]
M_s	$M_s(^\circ C) = 1350 - 1665(\%C + \%N) - 28\%Si - 33\%Mn - 42\%Cr - 61\%Ni$	Eichelmann, et al.	[88]
	$M_s(^\circ C) = 1182 - 1456(\%C + \%N) - 37\%Cr - 57\%Ni$	Monkman, et al.	[89]
	$M_s(^\circ C) = 492 - 125\%C - 65.5\%Mn - 10\%Cr - 29\%Ni$	Kulmburg, et al.	[90]
	$M_s(^\circ C) = 502 - 810\%C - 1230\%Ni - 13\%Mn - 30\%Ni - 12\%Cr - 54\%Cu - 46\%Mo$	Pickering	[91]
	$M_s(K) = 1578 - 41.7\%Cr - 61.1\%Ni - 33.3\%Mn - 27.8\%Si - 36.1\%Mo - 1667(\%C+\%N)$	Hammond	[92]
	$M_s(K) = A_3 - 199.8(\%C + 1.4\%N) - 17.9\%Ni - 21.7\%Mn - 6.8\%Cr - 45.0\%Si - 55.9\%Mo - 1.9(\%C + 1.4\%N)(\%Mo + \%Cr + \%Mn) - 14.4[(\%Ni + \%Mn)(\%Cr+\%Mo + \%Al+\%Si)]^{(1/2)} - 410$	Dai, et al.	[93]
	$M_s(K) = A_\varepsilon - 710.5(\%C + 1.4\%N) - 18.5\%Ni - 12.4\%Mn - 8.4\%Cr + 13.4\%Si - 1.6\%Mo - 22.7\%Al + 11.6(\%C + 1.4\%N)(\%Mo + \%Cr + \%Mn) - 3.7[(\%Ni + \%Mn)(\%Cr + \%Mo + \%Al + \%Si)]^{(1/2)} + 277$	Yuan, et al.	[94]
	$M_s(^\circ C) = 545 - 330\%C + 2\%Al + 7\%Co - 14\%Cr - 13\%Cu - 23\%Mn - 5\%Mo - 4\%Nb - 13\%Ni - 7\%Si + 3\%Ti + 4\%V + 0\%W$	Ishida	[95]
	$M_s(K) = 764.2 - 302.6\%C - 30.6\%Mn - 16.6\%Ni - 8.9\%Cr + 2.4\%Mo - 11.3\%Cu + 8.58\%Co + 7.4\%W - 14.5\%Si$	Capdevila, et al.	[96]

Table 3. Continued

	Formulae	Author	Ref.
M_{d30}	$M_s(\mathrm{K}) = 273 - 12.1\%\mathrm{Cr} - 17.7\%\mathrm{Ni} - 7.5\%\mathrm{Mo} - 423\%\mathrm{N}$	Xu, et al.	[97]
	$M_{d30}(^\circ\mathrm{C}) = 551 - 462(\%\mathrm{C} + \%\mathrm{N}) - 9.2\%\mathrm{Si} - 8.1\%\mathrm{Mn} - 13.7\%\mathrm{Cr} - 29(\%\mathrm{Ni} + \%\mathrm{Cu}) - 18.5\%\mathrm{Mo} - 68\%\mathrm{Nb}$	Nohara, et al.	[98]
	$M_{d30}(^\circ\mathrm{C}) = M_{d30}(\mathrm{Nohara} - 1.42 \times (\mathrm{GS} - 8)$ (GS means grain size according to ASTM)	Nohara, et al. (modified)	[98]
	$M_{d30}(^\circ\mathrm{C}) = 2462 - 14.4 \times \mathrm{GS} - 116.1\%\mathrm{Cr} - 134.1\%\mathrm{Mn}$ (GS means grain size according to ASTM)	Lewis, et al.	[99]
	$M_{d30}(^\circ\mathrm{C}) = 608 - 515\%\mathrm{C} - 812\%\mathrm{N} - 7.8\%\mathrm{Si} - 12\%\mathrm{Mn} - 13\%\mathrm{Cr} - 34\%\mathrm{Ni} - 6.5\%\mathrm{Mo}$	Sjöberg	[100]

Table 3. Empirical formulae for calculation the Nickel equivalent (Ni_{eq}), stacking fault energy (SFE), martensitic transformation temperature (M_s), martensitic transformation temperature (M_{d30}) as a function of chemical composition.

ε-martensite platelets. Therefore, the SFE is regarded as the sum of surface and volume energy contributions for the formation of ε-martensite in thermodynamic based models.[83] Chemical composition and temperature are the most critical factors that influence the SFE of austenite. The dependence of SFE on chemical composition is described by the various empirical formulae listed in Table 3. Table 3 also lists the empirical formula for calculating M_s and M_{d30} temperatures. M_s temperature is defined as the start temperature for martensitic transformation. M_{d30} defines the temperature at which an amount of 50% austenite will be transformed to martensite through cold deformation of 0.30 true strain.

Figure 5a reveals the microstructure evolution upon applied plastic deformation in an austenitic stainless steel 1.4301. Lath martensite was induced after 5% tensile deformation from the prior fully austenite microstructure. Cold rolling also induced martensitic transformation in meta-stable ASS.[101] As discussed before, α'-martensite nucleates in various lattice defects, Figure 5b displays the preferable α'-martensite nucleation sites in the intersections of deformation bands in a cast CrNiMn steel.[102]

The mechanical properties of meta-stable ASS reveal very strong temperature and strain rate dependency. Plastic deformation at lower temperature promotes the martensitic transformation and strengthens the material significantly.[103–106] **Figure 6**a shows the influence of temperature on the mechanical properties of grade 1.4301 after tensile testing in the temperature range 77–433 K.[106] The induced microstructure at the maximum uniaxial tensile stress was characterized by combined X-ray diffraction (XRD), optical microscopy study, and magnetic measurement, as shown in Figure 6b. Figure 6a reveals the strong temperature dependence of the flow curves below $M_d^{\gamma\to\alpha'}$ temperature, during which the $\gamma\to\alpha'$ transformation dominates. As revealed in Figure 6b, above the $M_d^{\gamma\to\alpha'}$ temperature, the ε-martensite phase increases continuously and the α'-martensite gradually diminishes. The maximum elongation is obtained at the start of the $\gamma\to\varepsilon\to\alpha'$ transformation temperature. Based on the results, the stress-temperature-transformation (STT) diagram with indicating the ranges of strain induced formation of ε- or α'-phase has been developed, as shown in Figure 6c. It gives

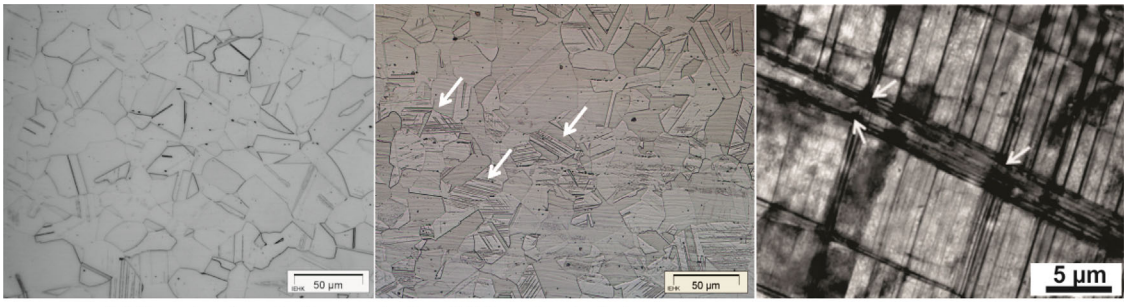

Figure 5. Microstructure of strain induced martensitic transformation in meta-stable austenitic stainless steels: a) Metallographic images steel grade 1.4301 before and after 5% tensile deformation. b) Transmission electron microscopy characterization of the transformed α' martensite at the intersections of deformation bands in a cast CrNiMn steel.[102]

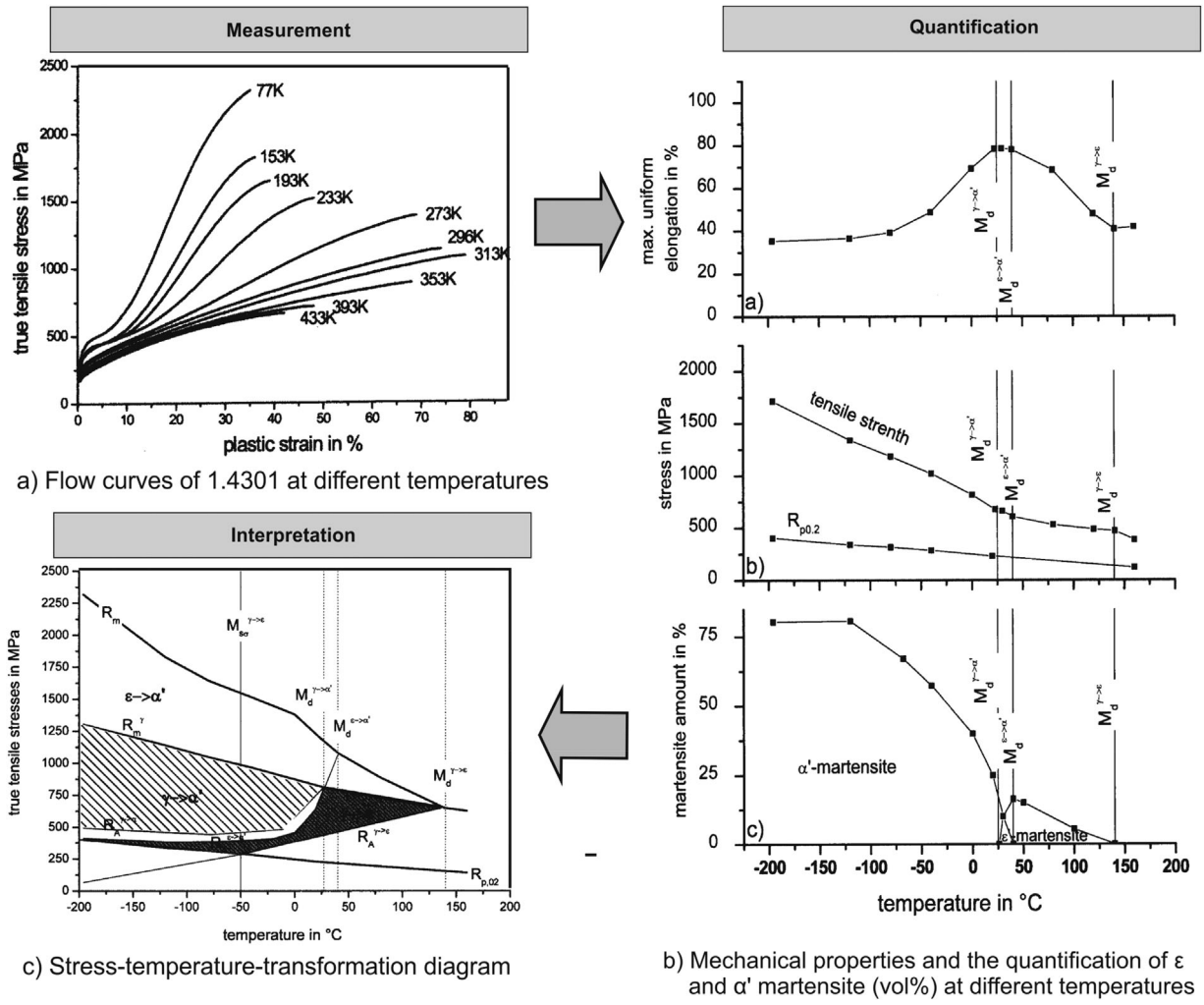

Figure 6. Influences of temperature on the mechanical properties and phase transformation in 1.4301 stainless steels: a) The flow curves of 1.4301 at different temperatures; b) The dependence of total elongation, tensile strength and martensitic volume fraction in 1.4301 at different temperatures; c) Stress–temperature transformation diagram that defines the transformation mechanisms in respective temperature and true stress range.[106]

guidance for the martensitic transformation mechanisms in accordance with applied stress and temperature. As the STT diagram is developed based on uniaxial tensile test, the transformation kinetics may differ when other stress states are applied.

Meta-stable ASS show a negative strain rate sensitivity, which means the tensile strength declines as the strain rate increases.[107,108] The main reason is that adiabatic heating at high strain rates reduces the chemical driving force for martensitic transformation.[109] The high strain rate may promote more irregular micro-shear band arrays and reduce the formation probability of α'-martensite embryos.[110] It is observed that high strain rates promote the formation of stacking faults and ε-martensite, however suppress α'-martensite in 1.4301.[111] **Figure 7**[108] reveals a systematic investigation on the mechanical behavior of steel grade 1.4318 at the strain rates between $6.0 \times 10^{-4}\,s^{-1}$ and $920\,s^{-1}$. As shown in Figure 7a, in the low strain rate region from $1.6 \times 10^{-4}\,s^{-1}$ to $0.8\,s^{-1}$, the negative strain rate sensitivity at high deformation strain is very pronounced. At strain rates above $0.8\,s^{-1}$, positive strain rate sensitivity is observed through the whole deformation range. It is assumed that the macroscopic flow stress σ can decompose into an athermal stress component σ_i, a thermally activated strain rate dependent positive dynamic stress offset $\Delta\sigma_{dynamic}$, as well as the transformation-induced flow stress increase $\Delta\sigma_{TRIP}$, as defined in Figure 7b. At strain rates above $0.8\,s^{-1}$, the adiabatic heating suppresses the TRIP effect. As a result, the flow stress is lower than the quasi-static strain rate conditions.

In summary, the meta-stable ASS have an excellent combination of strength and ductility, formability, and corrosion resistance. They are also cost competitive compared with other high Ni alloyed stable ASS due to the

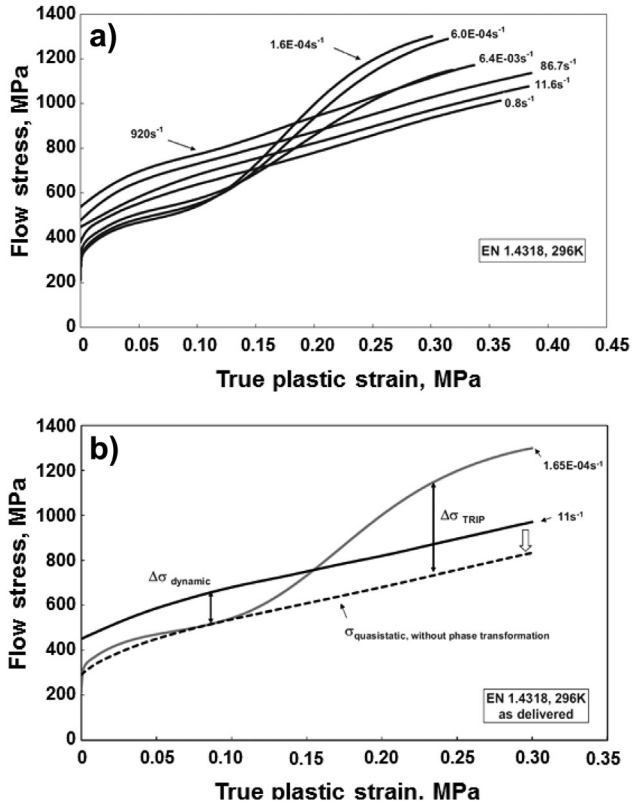

Figure 7. Influence of strain rate on the flow curves of a meta-stable ASS grade 1.4318: a) Flow curves at different strain rates; b) The contribution of dynamic stress offset $\Delta\sigma_{dynamic}$ and transformation stress offset $\Delta\sigma_{TRIP}$ on the macroscopic flow stress. The dashed line indicates the quasi–static flow stress without phase transformation.[108]

reduced Ni content. Therefore, they gain increasing interest to be utilized as strengthening parts, energy absorption component, which can also be exposed to corrosive environment. By controlling appropriate forming temperature, strain rate and strain path with consideration of austenite stability, the ultimate formability of meta-stable ASS can be exploited.

5. TRIP Effect in Low Carbon TRIP Steels

Different from high alloyed meta-stable ASS, low carbon TRIP steels contain typically 5–15 vol% retained austenite embedded in a matrix of ferrite, bainite, or martensite depending on alloy composition and production process. More carbon than that in conventional low carbon steels is added for stabilizing the retained austenite phase below ambient temperature. Si and/or Al are added to accelerate the ferrite/bainite formation and to postpone the carbide formation during the bainitic reaction.[112,113] As a result, carbon enriches in the retained austenite and the low carbon bainite is formed. The typical chemical compositions of commercialized TRIP steels are shown in **Table 4**.[114]

The strength of low carbon TRIP steels generally increases as the overall carbon concentration is raised. However, too high carbon contents have the drawback of retarding the bainitic transformation[115] and deteriorating the manufacturability such as welding.[116] The carbon concentration is not homogenous among the different phases in low carbon TRIP steels. The meta-stable austenite is enriched with carbon through the controlled two step intercritical annealing process. **Figure 8** illustrates the time–temperature processing routines for producing hot rolled and cold rolled TRIP steels.[117,118] The carbon enrichment occurs during the two phase (austenite + ferrite) intercritical annealing process step (780–880 °C) and the isothermal bainitic transformation step (350–500 °C).[119] Therefore, the M_s temperature of the retained austenite declines accordingly, leading to the stabilized retained austenite at room temperature.

In the past decades, many research activities took place to optimize the processing parameters of the intercritical annealing,[118,120,121] and of the subsequent isothermal bainitic transformation[122–124] to adapt the heat treatment production of TRIP steels to existing annealing and galvanizing lines.[26] In parallel, the effect of alloying elements on phase transformation, final microstructure, and induced mechanical properties has been intensively investigated.[121,125] Carbon is very crucial to raise the volume fraction and stability of retained austenite, and also has a strong solid solution strengthening effect. However, carbon contents beyond 0.2 wt% lead to detoriated weldability. Silicon is effective to postpone the carbide precipitation and ensures good stability of retained austenite. Since high silicon contents induce strong oxide layers and lead to poor coatability, silicon is partially replaced by Al, P, etc.[126,127] A schematic composition diagram summarizing the main reasons for the TRIP alloying concept is shown in **Figure 9**. In addition, Cu and Ni were found effective in

		Chemical composition, wt%				
Steel Designation	**Microstructure**	**C (max)**	**Si (max)**	**Mn (max)**	**P (max)**	**Al**
TRIP690	ferrite + bainite + retained austenite	0.24	2.00	2.20	0.050	0.015–2.0
TRIP780	ferrite + bainite + retained austenite	0.25	2.20	2.50	0.050	0.015–2.0

Table 4. Chemical composition of the commercial low carbon TRIP steels according to standard VDA 239-100.[114]

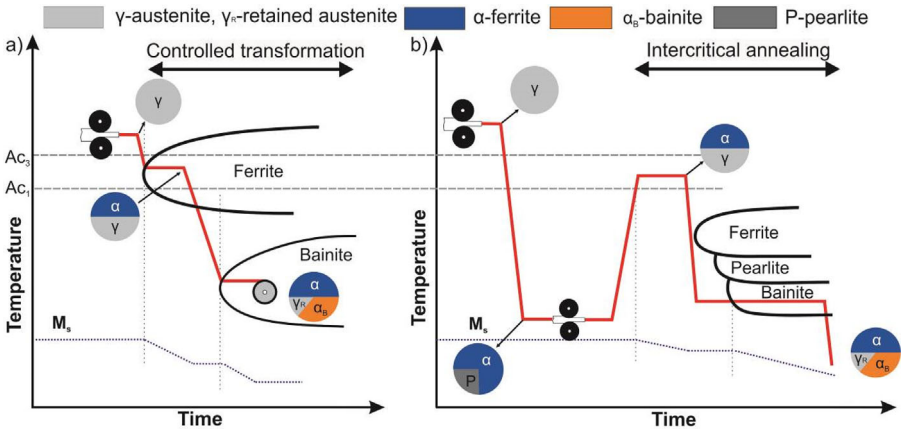

Figure 8. Processing routines to produce a) the hot rolled TRIP strips with controlled cooling after hot rolling and coiling in the bainitic transformation region and b) the cold rolled TRIP strips with intercritical annealing after cold rolling. The color disks denote the microstructure evolution.[117,118]

stabilizing the retained austenite, leading to the improvement in both strength and ductility.[128,129] Micro-alloying elements, such as Nb, Ti, and V were also added to achieve microstructure refinement and precipitation strengthening.[130–132]

All the steps above aim to achieve the desirable microstructure for the optimized mechanical properties. As a multiphase steel, the composite effect of soft ferrite phase for providing strain localization and hard bainite or martensite phase as strengthening phase for maintaining the excellent overall mechanical properties.[133] **Figure 10**a shows the schematic microstructural features of a TRIP steel and the important microstructure features that influence the mechanical properties. Among them, the volume fraction and stability of retained austenite play a great role in providing high strain-hardening coefficient (n-value).[123,134,135]

Figure 10b reveals the influences of austenite volume fraction and stability on the tensile properties of a 0.2C–1.8Mn–1.3Al–0.04Si–0.016P TRIP steel.[136] The material A has a higher stability ($M_S^{\sigma} = -15\,^{\circ}\mathrm{C}$) and a lower volume fraction of 11.3% γ_R by longer isothermal holding in the bainitic transformation region. It shows progressive transformation into martensite, which leads to the postponed occurring of necking. Material B has a lower austenite stability ($M_S^{\sigma} = -5\,^{\circ}\mathrm{C}$), which reveals higher instantaneous work hardening exponent at the start of deformation and leads to early fracture. The material A obtains improved fatigue performance (fatigue limit values = 478 MPa) compared with material B (fatigue limit values = 462 MPa) after 10^7 fatigue cycles, although A has lower ultimate tensile strength. The phase morphology also greatly influences the austenite stability. Figure 10c compares the austenite stability in a 0.17C–2.2Mn–1.6Al–0.013P TRIP steel with an equiaxed (material C) and a lamellar (material D) microstructure morphology.[137] A new processing routine with quenching the material below the M_s temperature before intercritical

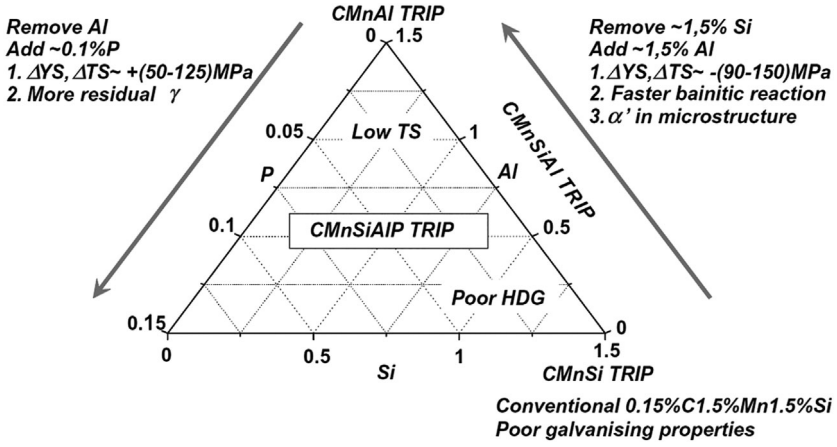

Figure 9. Schematic composition diagram for low alloy TRIP steels, showing the main reasons leading to the development of alternative compositions.[127]

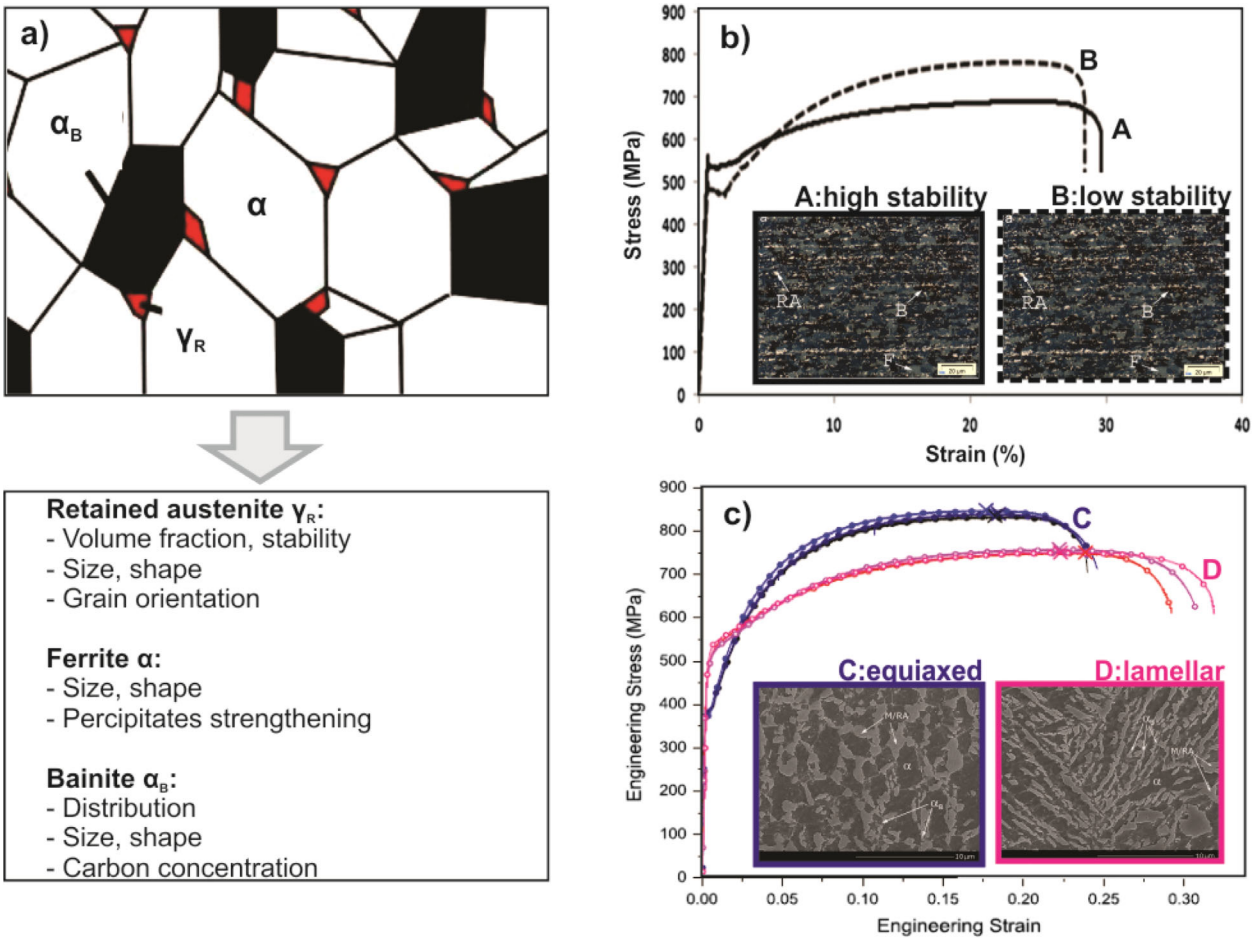

Figure 10. Important microstructure features influencing the mechanical properties of low carbon TRIP steels: a) The schematical microstructure of TRIP steels; b) The influences of austenite volume fraction and stability on the mechanical properties in a 0.2C–1.8Mn–1.3Al–0.04Si–0.016P TRIP steel[136]; c) The influences of the microstructure mophology on austenite stability and mechanical properties in a 0.17C–2.2Mn–1.6Al–0.013P TRIP steel.[137]

annealing produced the lamellar morphology in material D. In comparison to the equiaxed morphology in material C, the lamellar microstructure is more stable, which raises the value of total elongation by ≈10%. The ECO index has been raised from 20 400 to 23 100 MPa%.

Figure 11 compares the tensile properties between TRIP, Dual Phase (DP), and Complex Phase (CP) steels with the same strength level of 780 MPa. It reveals the TRIP 780 steel achieves obviously improved ductility and strain-hardening exponent compared with the other two grades. Much research work has also been carried out to improve the ductility of DP steels by introducing retained austenite, which is named as TRIP-assisted dual phase (TADP) steels.[138–141] In addition, most steel grades from the third-generation AHSS utilize the TRIP concept for achieving excellent combination of strength and ductility, which will be introduced in the following sections.

In summary, the low alloy concept and high strain-hardening capacity make low-carbon TRIP steels well suitable for automotive structural and safety parts such as cross members, longitudinal beams, B-pillar reinforcements and bumper reinforcements. With respect to cold formability, high spring back after press forming and poor stretch-flangeability of TRIP grades still need to be improved.[127,134]

6. TRIP Effect in High-Manganese Steels

The reduction in car-body weight and CO_2 emission and the improvement of crash safety in the automotive industry highly promote the development of the ultrahigh strength steels with superior ductility. The high-manganese TWIP (TWinning Induced Plasticity) and TRIP steels have attracted increasing interest by materials scientists and engineers since the last decades owing to their extraordinary mechanical performance.[30,31,143] It has been reported that the TRIP effect in high-manganese steels could result in superior mechanical properties, an

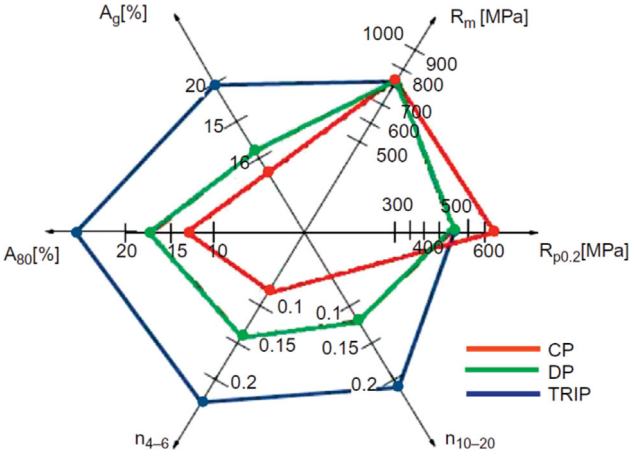

Figure 11. Tensile properties of CP, DP, and TRIP steel grades with the ultimate tensile strength level of 780 MPa. ($R_{p0.2}$ represents the 0.2% offset yield strength; R_m represents the ultimate tensile strength; A_g represents the uniform elongation; A_{80} represents the total elongation for a gauge length of 80 mm; n_{4-6} and n_{10-20} represent the strain-hardening exponent in the strain ranges of 4–6% and 10–20%, respectively).[142]

excellent combination of high strength and good ductility, and high strain-hardening capacity.[30,31] There are mainly three high-manganese steel groups, which have been intensively studied, namely Fe–Mn–Al–Si,[30,31,42,43,143–145] Fe–Mn–C,[146–148] and Fe–Mn–Al–C[149,150] alloys. The chemical composition and corresponding SFE of some typical high-manganese TRIP steels are listed in **Table 5**. The addition of Mn content higher than 15 wt% stabilizes the austenite phase. Consequently, high-manganese steels are composed of a single austenitic phase or of several phases with a large amount of austenite.

The superior mechanical properties of high-manganese steels benefit from various additional deformation mechanisms besides pure dislocation slip, such as TRIP effect, TWIP effect, and MBIP (MicroBand-Induced-Plasticity) effect. The SFE in high-manganese steels is a decisive parameter for the deformation mechanisms, which is a function of chemical composition and temperature. A thermodynamic SFE map for the Fe–Mn–Al–C system based on the sub-regular thermodynamic model was developed to explain the deformation mechanisms in high-manganese steels.[155] **Figure 12**a[152] displays the 2D SFE map of the Fe–Mn–C alloy system, which illustrates the chemical composition dependence of deformation mechanisms in high-manganese steels. The TRIP effect is believed to occur in high-manganese steels when a value of SFE is below 20 mJ m^{-2} and the TWIP effect is the dominant deformation mechanism when the SFE value is above 20 mJ m^{-2}. The strength of high-manganese TRIP steels lies in the range of 800–1000 MPa with large ductility in the range of 40–55%. During deformation, the meta-stable austenite can transform into ε- and/or α'-martensite,[29,156–159] effectively retarding stress localization and promoting homogeneous deformation. Figure 12b and c[152] show the EBSD image quality (IQ) maps of alloys Fe–13Mn–0.3C at strain 0.05 and Fe–22Mn–0.1C at strain 0.10, respectively. Additionally, the SFE values of Fe–13Mn–0.3C and Fe–22Mn–0.1C steels are marked in the 2D SFE map in Figure 12a. It can be seen that both steel grades are located in the TRIP region. As shown in Figure 12b, the γ-austenite in Fe–13Mn–0.3C alloy transforms into ε-martensite and α'-martensite during straining. However, there is only γ-austenite $\rightarrow$ ε-martensite transformation occurring in the Fe–22Mn–0.1C alloy during deformation, as illustrated in Figure 12c.

Because the SFE is a function of temperature as well, the deformation mechanisms in high-manganese steels are strongly affected by the deformation temperature. The temperature dependence of deformation modes has been studied in a Fe–17Mn–0.6C steel.[158] As shown in

	Chemical composition, wt%					
Steel Designation	**C**	**Si**	**Mn**	**Al**	**SFE, mJ m^{-2}**	**Ref.**
Fe–15Mn–3Al–3Si	n/a	2.80	15.99	3.08	n/a	[145]
Fe–19Mn–3Al–3Si	0.04	2.90	18.80	2.90	n/a	[43]
Fe–20Mn–2Al–3Si	0.03	3.30	19.93	2.12	n/a	[151]
Fe–13Mn–0.3C	0.30	n/a	13.00	n/a	≈0	[152]
Fe–17Mn–0.02C	0.02	2.87	17.22	0.48	n/a	[153]
Fe–18Mn–0.4C	0.44	0.33	17.40	0.01	14	[147]
Fe–22Mn–0.1C	0.10	n/a	22.00	n/a	7	[152]
Fe–14Mn–2Al–0.6C	0.64	0.25	14.00	2.40	n/a	[149]
Fe–18Mn–3Al–3Si–0.15C	0.15	3.26	18.40	3.01	n/a	[154]

n/a: not available.

Table 5. The chemical composition and stacking fault energy (SFE) of typical high-manganese TRIP steels.

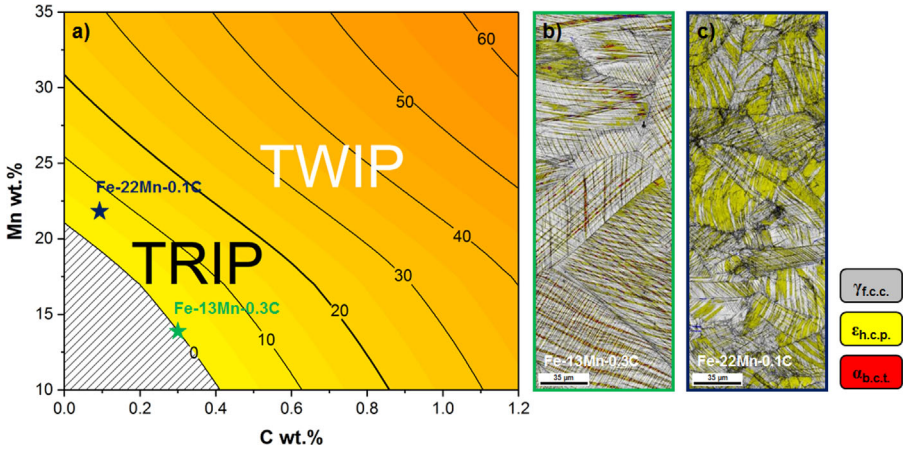

Figure 12. a) 2D SFE (unit, mJ m^{-2}) map of Fe–Mn–C high-manganese steels at 300 K[150]; EDSB IQ maps of b) Fe–13Mn–0.3C alloy at strain 0.05 and c) Fe–22Mn–0.1C alloy at strain 0.10.[152]

Figure 13a, the UTS shows very little change in this steel with different temperatures and the total elongation drops dramatically with the decrease in temperature. The corresponding strain-hardening rates tested at 173, 223, 294, and 373 K are shown in Figure 13b. It was proved by XRD that the ε-martensite appeared in the specimen deformed at 273 K and the intensity of it increased with the decrease in temperature.[158] No α'-martensite was observed.[158] Deformation induced twins were detected in the specimens deformed at 294 and 373 K by EBSD analysis.[158] It was claimed that the ε-martensite transformation could produce an extraordinary high strain-hardening rate of approximately 4 GPa at 10% strain.[158] By comparing the contribution of deformation twining and dynamic strain aging with the contribution of deformation-induced ε-martensite transformation to strain-hardening rate, it can be concluded that ε-martensite transformation has the highest contribution to the strain-hardening rate in Fe–Mn–C steel.[158]

Another study reported that by adjusting manganese content in Fe–Mn–C alloys, the SFE was reduced below 18 mJ m^{-2}, in the range where ε-martensite transformation is favorable instead of deformation-induced twins during deformation.[159] The ε-martensite was observed in these steels after tensile tests at room temperature. It was stated that the deformation-induced ε-martensite did not significantly deteriorate the mechanical properties of Fe–Mn–C steels.[159] The deformation-induced ε-martensite shows similar effects on the mechanical properties as twins. The progressive activation of two ε-martensite variants results in the reduction in the mean free path of the dislocation, consequently a high strain-hardening rate.[159] It was also mentioned that occurrence of deformation induced α'-martensite led to decreased ductility, due to its brittle characteristic.[159]

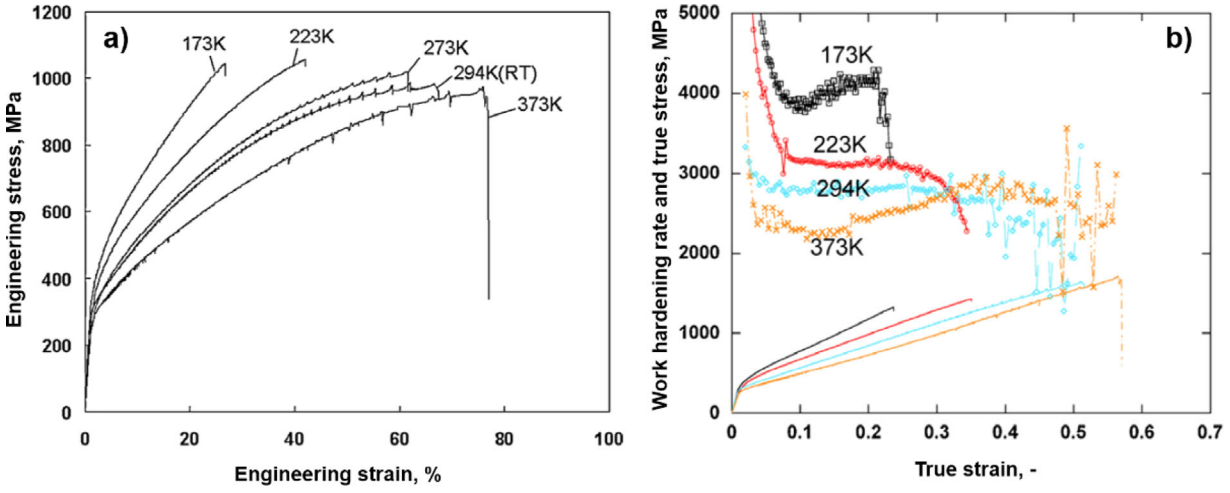

Figure 13. a) Engineering stress–strain curves and b) true stress–strain curves and corresponding strain–hardening rate of Fe–17Mn–0.6C steel at different temperatures.[158]

However, it is believed that the steel containing ε-martensite results in lower ductility than that of TWIP-assisted fully austenitic steel.[160] It has been found that cracks are prone to be initiated and propagated at the region of ε-martensite, which is normally harder than austenite.[160] In addition, ε-martensite provides a large amount of diffusible hydrogen trapping sites.[160] The γ/ε interface with low hydrogen trapping activation energy is responsible for the severe hydrogen embrittlement.[160] Although high-manganese austenitic TRIP steels show considerably high strain-hardening rate, the presence of strain-induced hard martensite phase deteriorates the in-service properties (e.g., hydrogen embrittlement) of steels strongly.

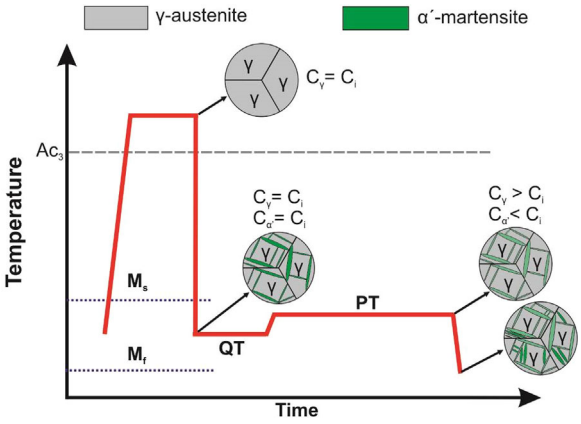

Figure 14. Schematic illustration of the Quenching and Partitioning (Q&P) process.[161] The light and dark green colors illustrate the martensite with different carbon contents.

7. TRIP Effect in Q&P Steels

The Q&P process enables to produce a novel martensite steel grade with good ductility; the process is illustrated in **Figure 14**.[161] Following austenitization, quenching is interrupted at a temperature (quenching temperature) in between of the M_s and M_f temperatures. At the quenching temperature martensite transformation is not completed and the quenching process results in quenched martensite and untransformed retained austenite.[162] Subsequently, a heat treatment is carried out at either the identical temperature to the quenching temperature, which is defined as one step Q&P process, or an evaluated temperature, which is referred to as two step Q&P process.[162] During the partitioning treatment process, carbon atoms diffuse from carbon-supersaturated martensite into the untransformed austenite. Consequently, carbon-enriched austenite can be retained when the steel is finally quenched to room temperature.

The Q&P steels take advantage of low alloying content. Mn, C, Al, and Si are the main alloying elements in Q&P steels. The chemical composition of several Q&P steels is listed in **Table 6**. Generally, C content is in a range of 0.15–0.3 wt%.[49] Mn content is controlled in between of 1.5–3.0 wt%.[49] Both C and Mn are austenite stabilizers. As the interstitial element in Q&P steels, C plays a critical role in stabilizing retained austenite during partitioning heat treatment. Si and/or Al are alloyed in Q&P steels to inhibit the cementite formation during partitioning process. The microstructure of Q&P steels consists of martensite, retained austenite, and ferrite (under partial austenitization condition). The quenching and partitioning process is expected to generate a fine acicular microstructure of lath martensite interwoven with carbon enriched retained austenite.[161] The microstructure of commercialized QP980 steel is composed of a certain amount of martensite (50–80 vol%) obtained during quenching, pro-eutectoid ferrite (20–40 vol%) formed from austenite during slow cooling, and dispersed retained austenite (5–10 vol%) stabilized by carbon enrichment during partitioning,[49] as shown in **Figure 15**. [163]

Compared with the ductility of the conventional martensitic steels, the Q&P steels can offer much higher ductility at the same strength level. The TRIP effect in retained austenite during plastic deformation contributes to the increase in strain hardening, improvement of UTS and uniform elongation.[165] Q&P steel grade can offer ultrahigh strength of 1000–1400 MPa with good ductility of 10–20%, which could be a promising candidate for

	Chemical composition, wt%						
Steel Designation	**C**	**Si**	**Mn**	**Al**	**N**	**V**	**Ref.**
Fe–2Mn–1.5Si–0.2C	0.20–0.22	1.40–1.67	1.65–2.04	n/a	n/a	0–0.2	[164–166]
Fe–3Mn–1.5Si–0.2C	0.20	1.60	3.00	0.06	0.0041	n/a	[167]
Fe–3Mn–1.5Si–0.3C	0.29	1.59	2.95	0.06	0.0039	n/a	[167]
Q&P (Baosteel)	0.15–0.30	1.00–2.00	1.50–3.00	0.02–0.06	n/a	n/a	[49]

n/a: not available.

Table 6. The chemical composition of typical Q&P steels.

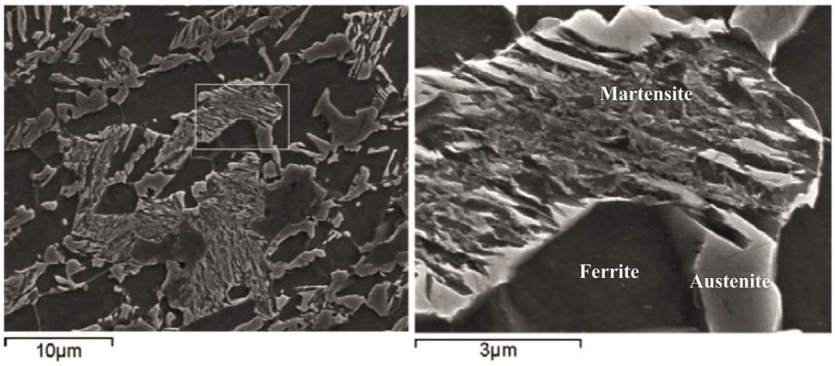

Figure 15. Microstructure of Q&P980 Fe–0.2C–1.5Si–1.8Mn.[163]

anti-intrusion barriers in automotive applications such as B-pillars, cross beams, front bumpers.[168] The mechanical properties of the commercialized Q&P980 steel show a tensile strength of 980 MPa with adequate total elongation of approximately 20%.[49]

Recently, the phase transformation kinetics of deformation-induced martensite in the commercialized Q&P980 steel was studied by in situ synchrotron X-ray diffraction (SYXRD) during tensile tests.[169] **Figure 16**a[169] shows the engineering stress–engineering strain curves of three Q&P980 specimens. The UTS is about 990 MPa and TEL is around 25%.[169] The austenite fraction was analyzed by SYXRD profile fitting.[169] The evolution of austenite phase during tensile tests is illustrated in Figure 16b. The initial austenite fraction prior to tensile tests is around 0.115. During deformation, the austenite progressively transforms into α'-martensite and the austenite fraction declines to 0.04–0.05 at the end of deformation.[169] The TRIP effect contributes to the enhanced strain-hardening rate and improved ductility in martensitic steels.

Taking the advantage of the TRIP effect in retained austenite during deformation, Q&P steels exhibit a good combination of high strength and adequate ductility for anti-intrusion applications in automotive industry. The specific heat treatment cycle (Q&P process) leads to retaining austenite down to room temperature without necessity of high alloying. However, Q&P process is a complex process, which integrates austenitization step, controlled quenching step, and partitioning step. The heat treatment parameters need to be adjusted properly to achieve desired microstructure and mechanical properties. The feasibility of this two-step heat treatment in currently available continuous annealing lines needs to be further explored.

8. TRIP Effect in Medium-Manganese Steels

The medium-manganese TRIP steels are processed by intercritical annealing in between A_1 and A_3 temperatures, which is also named Austenite-Reverted-Transformation (ART) annealing.[170] The heat treatment cycle of medium-manganese TRIP steels consists of

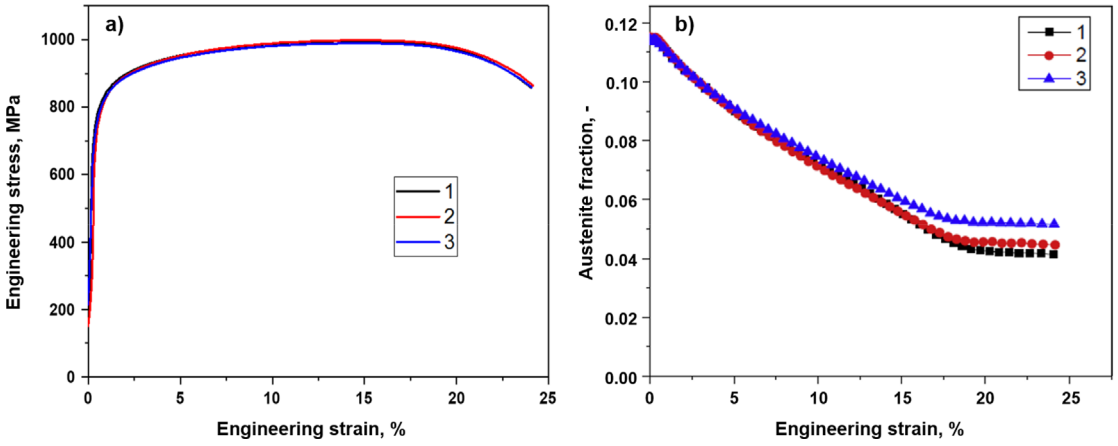

Figure 16. a) Engineering stress–engineering strain curve and b) retained austenite fraction as a function of engineering strain from in situ tensile tests of three Q&P980 specimens tracked by synchrotron XRD.[169] The test has been repeated with three samples, designated 1, 2, and 3 in the figure.

austenitization and ART annealing. Before ART annealing, the steel strip is heated above A_3 temperature to achieve a fully austenitic microstructure. Subsequently, the austenite transforms to athermal α'-martensite by quenching to room temperature. Alternatively, the conventional rolling and ART-annealing process might be employed to manufacture this steel grade. Hot rolling is possibly conducted above the A_3 temperature combined with an austenitization treatment. During the cold rolling process, some retained austenite from hot rolled medium-manganese steels might transform into martensite. Afterwards, the cold-rolled steel strip is reheated to the intercritical annealing region between A_1 and A_3, and maintained at this evaluated temperature for some time, followed by cooling to room temperature, as shown in **Figure 17**. During ART annealing, the nucleation of austenite takes place along martensite lath boundaries, martensite block boundaries or primary austenite boundaries,[171] leading to a pronounced grain refinement.[172,173] By ART annealing, austenite is enriched in C and Mn. It is believed that the Mn partitioning at the martensite/austenite interface results in the formation and growth of austenite.[39,174] The diffusion of Mn by small distance during ART annealing in the UFG steels enables a certain amount of retained austenite.[175]

As a consequence of ART annealing, either UFG duplex microstructures with austenite and ferrite lamella,[176,177] or equiaxed microstructures with ferrite and retained austenite are obtained in medium-manganese steels.[177] The resulting UFG microstructure yields a grain size smaller than 1 μm,[176,178] which effectively raises the thermal stability of retained austenite.[50] It was documented that the hot rolled Fe–9Mn–0.05C steel had a lamella microstructure of elongated lath-shaped ferrite (α_L) and austenite (γ_L) phases after ART annealing, while the cold rolled Fe–9Mn–0.05C steel shows an equiaxed microstructure of globular-shaped ferrite (α_G) and austenite (γ_G) phases, as shown in **Figure 18**.[33,53] It was pointed out that the initial microstructure of hot rolled Fe–9Mn–0.05C steel was full athermal martensite, however the microstructure of the cold rolled Fe–9Mn–0.05C steel was deformed martensite.[33] During ART annealing, recovery

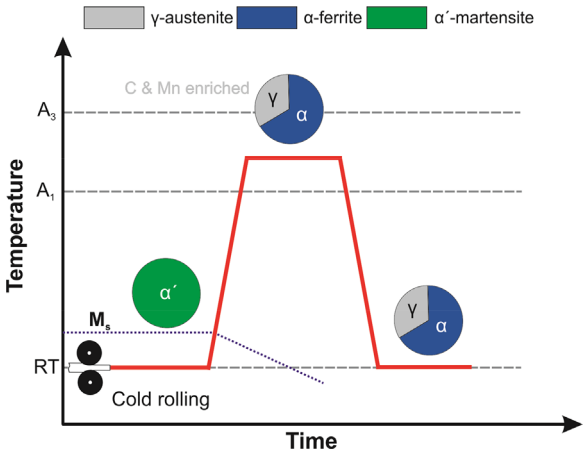

Figure 17. Schematic representation of ART-annealing process.

in the hot rolled steel is sluggish. On the contrary, the recovery and recrystallization takes place in cold rolled steel during ART annealing.[33]

The main alloying elements in medium-manganese steels are Mn, C, Al, and Si. Mn and C are strong austenite stabilizers. In medium-manganese steels, Mn is the most important alloying element, which can effectively stabilize the austenite phase.[172] It usually contains 4–12 wt% manganese in medium-manganese steels. The C content is generally around 0.05–0.4 wt%. Al and Si are around 1.5–3.0 wt% and 1.2–2.0 wt%, respectively. On the one hand, Al and Si can prevent carbide formation during ART annealing; on the other hand, the addition of Al and Si shifts the intercritical annealing temperature window to higher temperatures, allowing a faster kinetics of austenite reverted transformation.[179] The chemical composition of some typical medium-manganese steels are listed in **Table 7**.

To understand the deformation mechanisms is of great importance to evaluate the mechanical properties in UFG duplex medium-manganese steels. A study of Fe–5Mn–0.2C steel reported that during deformation there was no apparent change of the ferrite phase apart from the slight increase in dislocation density.[184] However,

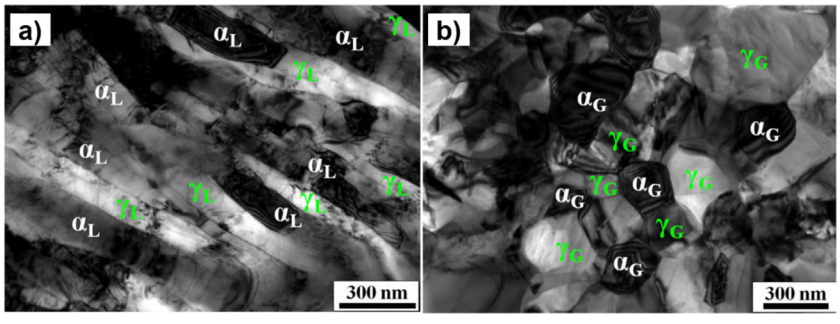

Figure 18. Bright filed TEM images of Fe–9Mn–0.05C medium-manganese steels after annealing at 620 °C for 10 min: a) hot rolled specimen and b) cold rolled specimen.[33]

Steel Designation	Chemical composition, wt%							Ref.
	C	Si	Mn	Cr	Al	N	V	
Fe–4.5Mn–0.2C	0.20	0.15	4.50	0.1	0.028	n/a	n/a	[180]
Fe–5Mn–0.2C	0.21	1.50	4.94	n/a	0.032	0.002	n/a	[181]
Fe–6Mn–0.05C	0.05	1.50	6.15	n/a	n/a	n/a	n/a	[50]
Fe–8Mn–0.1C	0.07	0.14	7.90	n/a	0.05	n/a	n/a	[182]
Fe–8Mn–0.4C–(0.2V)	0.40	2.00	8.00	n/a	3.00	n/a	0-0.2	[172]
Fe–9Mn–0.05C	0.05	0.29	8.51	n/a	0.08	n/a	n/a	[178]
Fe–9Mn–0.2C	0.17	n/a	9.00	n/a	3.50	n/a	n/a	[183]

Table 7. The chemical composition of typical medium-manganese steels. (n/a: not available)

the α'-martensite phase transformation was characterized in UFG austenite phase during deformation by XRD. The XRD measurements revealed a continuous decrease of austenite fraction from 40–0.6 vol% with progressive straining up to 30%, indicating the complete phase transformation of austenite to α'-martensite.[184] Moreover, XRD results confirmed the absence of ε-martensite transformation as a transition phase.[184] Recently, it was found that intercritically annealed 10 wt% Mn steels exhibited excellent mechanical properties with tensile strength up to 1144 MPa and elongation about 65%.[185] The high strain-hardening rate of this steel was reported to be related to the combination of TWIP and TRIP effect occurring progressively during the tensile test.[185] During mechanical deformation primary twins are generated and followed by secondary twins.[185] The twin intersections are expected to be the nucleation sites for the following deformation induced α'-martensite transformation.[185]

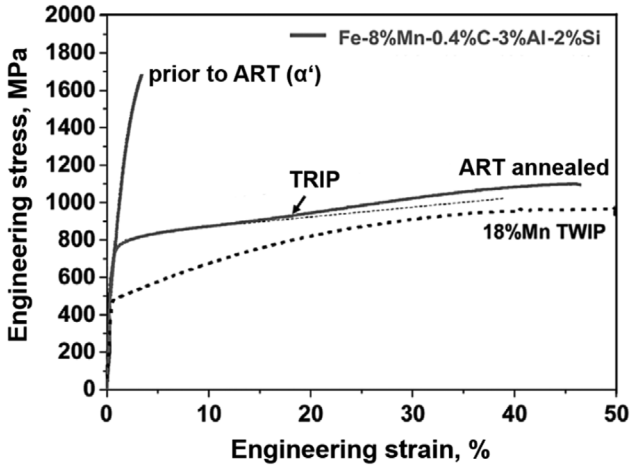

Figure 19. Mechanical properties of Fe–8Mn–0.4C–3Al–2Si steel prior to ART annealing and after ART annealing. The stress–strain curve of high-manganese TWIP steel is shown for comparison. The upward curvature in the stress–strain curves is marked by the arrows, indicating the activation of the TRIP effect.[172]

Figure 19 displays the mechanical properties of Fe–8Mn–0.4C–3Al–2Si steel prior to the ART annealing and after the ART annealing.[172] It can be seen that the ductility is effectively improved after the ART annealing. The high strain-hardening rate of this steel is related to the combination of TWIP and TRIP effect occurring progressively during the tensile test.[172] Because austenite is enriched in Mn and C after ART annealing, the SFE of austenite phase could achieve the level high enough to promote deformation twins. As mentioned previously, primary twins generate first and are followed by secondary twins at the early stage of deformation. Then, deformation induced α'-martensite nucleates at the twin intersections,[172] which further strengthens the material and improves the strain-hardening capacity of the steel. The change of the curvature in the stress–strain curve is illustrated by the arrows in Figure 19, which indicates the activation of the TRIP effect.[172]

The TRIP effect enhances the strain-hardening rate and ductility in medium-manganese steels. However, the appearance of the localized deformation behavior in medium-manganese steels is still not well understood. Furthermore, for the industrialization and application of medium-manganese steels, there are lots of properties required to be further evaluated, like weldability, hole expansion ratio, sheet formability (forming limit diagram), dynamic tensile properties, delayed fracture properties, and impact toughness etc.[33–35] The two-step heat treatment process for medium-manganese steels might not be compatible with the present steel processing routes. An upgrade of the equipment to achieve two-step annealing may be necessary.

9. Conclusions

The positive impact of a martensitic phase transformation on the ductility of steels has been observed already in the

1930's, the first ideas to make technical use of this effect date back to the 1950's with a focus on austenitic stainless steels. The search for low alloyed high strength steels with improved formability in the 1980's became the nucleus for the development of the low carbon TRIP steels; now only a part of the microstructure is affected by the TRIP related phase transformations. This new idea of using the TRIP phenomenon in multiphase microstructures fostered new steel concepts in recent years.

The availability of continuous annealing lines (and modern hot-dip galvanizing lines) with accurate temperature-time control and the option for high cooling rates stimulated new ideas for complex heat treatments in order to create mixtures of different phases with well-defined morphologies and local element enrichments by partitioning. In most steels, it is the C enrichment, that is, decisive for the retained austenite stability. New observations also indicate that in nanostructured steels Mn enrichment by small distance diffusion contributes to the stability control beside morphological effects. This retained austenite stability is decisive for the smoothness of transformation during the forming processes.

While the principles for steel design using the TRIP effect seem to be well understood, the process layout is still a matter of discussion. The parameter windows and the sensibility to small parameter changes for many new steel concepts are in contradiction to the industrial need for robust processes. Finally, it should be mentioned that most laboratory studies related to the development of TRIP-aided steels are based on experiments using the uniaxial tensile test, while in real forming processes multiaxial stress states and changing strain paths are characteristic. Simulation tools for the impact of different stress states and strain paths on the TRIP behavior, as well as damage mechanics oriented new research approaches will be necessary for the further successful application of TRIP steels.

Acknowledgements

Part of this review work is supported by Deutsche Forschungsgemeinschaft (DFG) in the framework of the Collaborative Research Center SFB 761 'Steel-*ab initio*: quantum mechanics guided design of new Fe based materials', which is gratefully acknowledged.

Received: May 24, 2017; Revised: July 18, 2017; Published online: August 10, 2017

Keywords: cold formable sheet steels; mechanical properties; microstructure; process design; transformation-induced plasticity

References

[1] V. F. Zackay, E. R. Parker, D. Fahr, R. Bush, *Trans. Am. Soc. Met.* **1967**, *60*, 252.
[2] X. Guo, J. Post, M. Groen, W. Bleck, *Steel Res. Int.* **2011**, *82*, 6.
[3] E. Scheil, *Z. Anorg. Allg. Chem.* **1929**, *183*, 98.
[4] E. Scheil, *Z. Anorg. Allg. Chem.* **1932**, *207*, 21.
[5] G. Wassermann, *Arch. Eisenhüttenwesen* **1933**, *6*, 347.
[6] G. Wassermann, *Arch. Eisenhüttenwesen* **1937**, *11*, 89–93.
[7] A. K. Richard, W. Volker, *Metall. Trans.* **1970**, *1*, 2685.
[8] J. R. Patel, M. Cohen, *Acta Metall.* **1953**, *1*, 531.
[9] E. Houdremont, O. Krisement, *Arch. Eisenhüttenwesen* **1953**, *24*, 53.
[10] E. Scheil, *Arch. Eisenhüttenwesen* **1959**, *30*, 751.
[11] F. Lihl, J. Thöny, *Arch. Eisenhüttenwesen* **1963**, *34*, 701.
[12] K. Bungardt, W. Spyra, A. von den Steinen, *Arch. Eisenhüttenwesen* **1968**, *39*, 719.
[13] E. W. H. Kimmich, *Arch. Eisenhüttenwesen* **1964**, *35*, 1193.
[14] E. Schmidtmann, L. Elsing, H. Schenck, *Arch. Eisenhüttenwesen* **1965**, *36*, 415.
[15] W. Jellinghaus, O. Schmidt, *Arch. Eisenhüttenwesen* **1965**, *36*, 677.
[16] E. Scheil, *Arch. Eisenhüttenwesen* **1956**, *27*, 801.
[17] V. F. Zackay, E. R. Parker, *U.S. Patent 3488231* **1970**.
[18] D. Fahr, *Metall. Trans.* **1971**, *2*, 1883.
[19] O. Matsumura, Y. Sakuma, H. Takechi, *Trans. Iron Steel Inst.* **1987**, *27*, 570.
[20] H. Takechi, O. Matsumura, Y. Sakuma, *Jpn. Kokai Tokyo Koho Jpn. Patent 62* **1987**, *188*, 729.
[21] Y. Sakuma, O. Matsumura, O. Akisue, *ISIJ Int.* **1991**, *31*, 1348.
[22] K.-I. Sugimoto, M. Kobayashi, S.-I. Hashimoto, *Metall. Trans. A* **1992**, *23*, 3085.
[23] K.-I. Sugimoto, M. Misu, M. Kobayashi, H. Shirasawa, *ISIJ Int.* **1993**, *33*, 775.
[24] O. Matsumura, Y. Sakuma, H. Takechi, *ISIJ Int.* **1992**, *32*, 1014.
[25] D. Cornette, T. Hourman, O. Hudin, J. P. Laurent, A. Reynaert, High strength steels for automotive safety parts. No. 2001-01-0078. SAE Tech. Paper **2001**.
[26] N. Fonstein, *Advanced High Strength Sheet Steels: Physical Metallurgy, Design, Processing, and Properties*, Springer International Publishing, New York City **2015**.
[27] S. Keeler, M. Kimchi, *Advanced High-Strength Steel Application Guidelines Version 5.0*, WorldAutoSteel, Ohio **2014**.
[28] C. H. White, R. W. K. Honeychombe, *J. Iron Steel Inst.* **1962**, *200*, 457.
[29] Y. Tomota, M. Strum, J. W. Morris, *Metall. Trans. A* **1986**, *17*, 537.
[30] O. Grässel, G. Frommeyer, C. Derder, H. Hofmann, *J. Phys. IV* **1997**, *07*, C5-383-C5-388.
[31] U. Brüx, G. Frommeyer, O. Grässel, L. W. Meyer, A. Weise, *Steel Res. Int.* **2002**, *73*, 294.

[32] J. G. Speer, D. K. Matlock, B. C. De Cooman, J. G. Schroth, *Acta Mater.* **2003**, *51*, 2611.
[33] Y.-K. Lee, J. Han, *Mater. Sci. Technol.* **2015**, *31*, 843.
[34] D.-W. Suh, S.-J. Kim, *Scr. Mater.* **2017**, *126*, 63.
[35] Y. Ma, *Mater. Sci. Technol* **2017**, DOI: 10.1080/02670836.2017.1312208.
[36] R. L. Miller, *Metall. Mater. Trans. B* **1972**, *3*, 905.
[37] D. Raabe, D. Ponge, O. Dmitrieva, B. Sander, *Adv. Eng. Mater.* **2009**, *11*, 547.
[38] D. Raabe, D. Ponge, O. Dmitrieva, B. Sander, *Scr. Mater.* **2009**, *60*, 1141.
[39] O. Dmitrieva, D. Ponge, G. Inden, J. Millán, P. Choi, J. Sietsma, D. Raabe, *Acta Mater.* **2011**, *59*, 364.
[40] Z. Li, K. G. Pradeep, Y. Deng, D. Raabe, C. C. Tasan, *Nature* **2016**, *534*, 227.
[41] S. Hoffmann, W. Bleck, B. Berme, *Steel Res. Int.* **2012**, *83*, 379.
[42] D. P. Escobar, S. S. F. de Dafe, K. Verbeken, D. B. Santos, *Steel Res. Int.* **2016**, *87*, 95.
[43] H. Ding, H. Ding, X. Zhang, Z. Tang, P. Yang, *Steel Res. Int.* **2009**, *80*, 623.
[44] A. Arlazarov, O. Bouaziz, J. P. Masse, F. Kegel, *Mater. Sci. Eng. A* **2015**, *620*, 293.
[45] A. Arlazarov, M. Ollat, J. P. Masse, M. Bouzat, *Mater. Sci. Eng. A* **2016**, *661*, 79.
[46] W. Feng, Z. Wu, L. Wang, J. G. Speer, *Steel Res. Int.* **2013**, *84*, 246.
[47] S. Li, D. Zou, C. Xia, J. He, *Steel Res. Int.* **2016**, *87*, 1302.
[48] J. Sun, H. Yu, *Mater. Sci. Eng. A* **2013**, *586*, 100.
[49] L. Wang, J. G. Speer, *Metall. Microstruct. Anal.* **2013**, *2*, 268.
[50] S. Lee, S. J. Lee, K. S. Santhosh, K. Lee, B. C. de Cooman, *Metall. Mater. Trans. A* **2011**, *42*, 3638.
[51] P. J. Gibbs, E. de Moor, M. J. Merwin, B. Clausen, J. G. Speer, D. K. Matlock, *Metall. Mater. Trans. A* **2011**, *42*, 3691.
[52] A. Arlazarov, M. Gouné, O. Bouaziz, A. Hazotte, G. Petitgand, P. Barges, *Mater. Sci. Eng. A* **2012**, *542*, 31.
[53] J. Han, S.-J. Lee, J.-G. Jung, Y.-K. Lee, *Acta Mater.* **2014**, *78*, 369.
[54] J. Han, J. H. Nam, Y. K. Lee, *Acta Mater.* **2016**, *113*, 1.
[55] Z. Li, C. C. Tasan, H. Springer, B. Gault, D. Raabe, *Sci. Rep.* **2017**, *7*, 40704.
[56] Z. Li, C. C. Tasan, K. G. Pradeep, D. Raabe, *Acta Mater.* **2017**, *131*, 323.
[57] *World Auto Steel*, http://www.worldautosteel.org/steel-basics/steel-types/transformation-induced-plasticity-trip-steel/ **2017**.
[58] DIN EN 10088-2: 2014, Stainless steels - Part 2: Technical delivery conditions for sheet/plate and strip of corrosion resisting steels for general purposes.
[59] Z. Nishiyama, *Martensitic Transformation*, Academic Press, New York **1978**.
[60] E. C. Bain, N. Y. Dunkirk, *Trans. AIME* **1924**, *70*, 25.
[61] G. V. Kurdjumov, G. Sachs, *Z. Phys.* **1930**, *64*, 325.
[62] P. M. Kelly, in *Phase Transformations in Steels: Volume 2: Diffusionless Transformations, High Strength Steels, Modelling and Advanced Analytical Techniques* (Eds: E. Pereloma, D. V. Edmonds), Woodhead Publishing Limited, Cambridge, UK **2012**, p. 3.
[63] G. B. Olson, M. Cohen, *J. Less-Common Met.* **1972**, *28*, 107.
[64] G. F. Bolling, R. Richman, *Scr. Metall.* **1969**, *6*, 365.
[65] G. B. Olson, M. Cohen, *Metall. Mater. Trans. A* **1975**, *6*, 791.
[66] K. H. Lo, C. H. Shek, J. K. L. Lai, *Mater. Sci. Eng. R: Rep.* **2009**, *65*, 39.
[67] A. Das, S. Sivaprasad, M. Ghosha, P. C. Chakraborti, S. Tarafder, *Mater. Sci. Eng. A* **2008**, *486*, 283.
[68] T. Kruml, J. Polak, S. Degallaix, *Mater. Sci. Eng. A* **2000**, *293*, 275.
[69] W. S. Lee, C. F. Lin, *Scr. Mater.* **2000**, *43*, 777.
[70] J. Y. Choi, W. Jin, *Scr. Mater.* **1997**, *36*, 99.
[71] P. Hedström, U. Lienert, J. Almer, M. Odén, *Scr. Mater.* **2007**, *56*, 213.
[72] K. Spencer, M. Véron, K. Yu-Zhang, J. D. Embury, *Mater. Sci. Technol.* **2009**, *25*, 7.
[73] T. Angel, *J. Iron Steel Inst.* **1954**, *177*, 165.
[74] E. S. Perdahcıoğlu, H. J. M. Geijselaers, in *Proc. of the 10th Int. Conf. on Technology of Plasiticity, ICTP2011* (Eds: Gerhard Hirt, A. Erman Tekkaya), Verl. Stahleisen GmbH, Düsseldorf **2011**, p. 685.
[75] R. G. Stringfellow, D. M. Parks, G. B. Olson, *Mater. Sci. Eng.* **1992**, *40*, 1703.
[76] T. Iwamoto, T. Tsuta, Y. Tomita, *Int. J. Mech. Sci.* **1998**, *40*, 173.
[77] P. O. Santacreu, J. C. Glez, G. Chinouilh, T. Frohlich, *Steel Res. Int.* **2006**, *77*, 686.
[78] V. G. Kouznetsova, M. Geers, *Mech. Mater.* **2008**, *40*, 641.
[79] S. Traint, A. Pichler, K. Hauzenberger, P. Stiaszny, E. Werner, *Steel Res.* **2002**, *73*, 259.
[80] S. Gupta, R. Twardowski, P. Kucharczyk, S. Münstermann, *Steel Res. Int.* **2014**, *85*, 793.
[81] R. E. Schramm, R. Reed, *Metall. Trans. A* **1975**, *6*, 1345.
[82] P. J. Ferreira, P. Müllner, *Acta Mater.* **1998**, *46*, 4479.
[83] G. B. Olson, M. Cohen, *Metall. Trans. A* **1976**, *7*, 1897.
[84] C. G. Rhodes, A. Thompson, *Metall. Mater. Trans. A* **1977**, *8*, 1901.
[85] T. Takemoto, Y. Murata, T. Tanaka, *ISIJ Int.* **1990**, *30*, 608.
[86] F. B. Pickering, in *Stainless Steels '84: Proc. of the Conf.* (Ed: C. T. Högskola), Institute of Metals, London **1984**, p. 2.
[87] Q. X. Dai, A. D. Wang, X. N. Cheng, X. M. Luo, *Chin. Phys.* **2002**, *11*, 596.
[88] G. H. Eichelmann, F. C. Hull, *Metall. Mater. Trans. A* **1953**, *45*, 77.

[89] F. C. Monkman, F. B. Cuff, N. J. Grant, *Met. Prog.* **1957**, *71*, 94.
[90] A. Kulmburg, W. Sölkner, F. Korntheuer, H. E. Schmidt, *Berg-u. hüttenm. Mh* **1979**, 400.
[91] F. B. Pickering, *Physical Metallurgy and the Design of Steels*, Applied Science Publishers, London **1978**.
[92] C. M. Hammond, *Cobalt* **1964**, *25*, 195.
[93] Q. X. Dai, X. N. Cheng, Y. T. Zhao, X. M. Luo, Z. Z. Yuan, *Mater. Charact.* **2004**, *52*, 349.
[94] Z. Z. Yuan, Q. X. Dai, Q. Zhang, X. N. Cheng, K. M. Chen, *Mater. Charact.* **2008**, *59*, 18.
[95] K. Ishida, *J. Alloys Compd.* **1995**, *1*, 126.
[96] C. Capdevila, F. G. Caballero, C. G. De Andrés, *ISIJ Int.* **2002**, *42*, 894.
[97] W. Xu, P. E. J. Rivera-Díaz-del-Castillo, S. van der Zwaag, *Comput. Mater. Sci.* **2008**, *44*, 678.
[98] K. Nohara, Y. Ono, N. Ohashi, *J. Iron Steel Inst. Jpn.* **1977**, *63*, 212.
[99] D. T. Lewis, J. G. Speer, D. K. Matlock, M. C. Mataya, *Iron Steel Soc.* **1999**, *37*, 343.
[100] J. Sjöberg, *Wire* **1973**, *23*, 155.
[101] A. Hedayati, A. Najafizadeh, A. Kermanpur, F. Forouzan, *J. Mater. Process. Technol.* **2010**, *210*, 1017.
[102] A. Glage, A. Weidner, H. Biermann, *Steel Res. Int.* **2011**, *82*, 1040.
[103] X. F. Fang, W. Dahl, *Mater. Sci. Eng. A* **1991**, *141*, 189.
[104] G. L. Huang, D. K. Matlock, G. Krauss, *Metall. Trans. A* **1989**, *20*, 1239.
[105] T. S. Byun, N. Hashimoto, K. Farrell, *Acta Metall.* **2004**, *52*, 3889.
[106] A. Weiß, H. Gutte, P. R. Scheller, *Steel Res. Int.* **2006**, *77*, 727.
[107] L. Krüger, S. Wolf, S. Martin, U. Martin, A. Jahn, A. Weiß, P. R. Scheller, *Steel Res. Int.* **2011**, *82*, 1087.
[108] P. Larour, P. Verleysen, K. Dahmen, W. Bleck, *Steel Res. Int.* **2013**, *84*, 72.
[109] G. W. Powell, E. R. Marshall, W. A. Backofen, *Metall. Mater. Trans. A* **1958**, *50*, 478.
[110] K. P. Staudhammer, L. E. Murr, S. S. Hecker, *Acta Metall.* **1983**, *31*, 267.
[111] P. J. Ferreira, J. B. V. Sande, M. A. Fortes, A. Kyröläinen, *Metall. Mater. Trans. A* **2004**, *35*, 3091.
[112] L. Zhao, J. Sietsma, S. van der Zwaag, *ISIJ Int.* **2002**, *42*, 1565.
[113] A. Mertens, P. J. Jacques, J. Sietsma, F. Delannay, *Steel Res. Int.* **2008**, *79*, 954.
[114] *VDA 239-100 Flacherzeugnisse aus Stahl zur Kaltumformung*, Verband der Automobilindustrie e. V. **2016**.
[115] K. Lee, Y. R. Im, K. G. Chin, *Mater. Sci. Technol.* **2008**, *6–9*, 1785.
[116] C. Laurent, K. Ali Ihsan, T. M. Lucía, *Steel Res. Int.* **2002**, *73*, 314.
[117] Y. Sakuma, N. Kimura, A. Itami, S. Hiwatashi, O. Kawano, K. Sakata, *Nippon Steel Tech. Rep.* **1995**, *64*, 20.
[118] H. Matsuda, F. Kitano, K. Hasegawa, T. Urabe, Y. Hosoya, *Steel Res.* **2002**, *73*, 211.
[119] J. Zrnik, I. Mamuzić, S. V. Dobatkin, *Metalurgija* **2006**, *45*, 323.
[120] K. Eberle, P. Cantinieaux, P. Harlet, *Steel Res. Int.* **1999**, *70*, 233.
[121] A. Pichler, P. Stiaszny, *Steel Res. Int.* **1999**, *70*, 459.
[122] T. lung, J. Drillet, A. Couturier, C. Olier, *Steel Res. Int.* **2002**, *73*, 218.
[123] A. N. Vasilakos, K. Papamantellos, G. N. Haidemenopoulos, W. Bleck, *Steel Res.* **1999**, *70*, 466.
[124] S. M. K. Hosseini, A. Zarei-Hanzaki, S. Yue, *Steel Res. Int.* **2016**, *87*, 146.
[125] P. J. Jacques, E. Girault, A. Mertens, B. Verlinden, J. van Humbeeck, F. Delannay, *ISIJ Int.* **2001**, *41*, 1068.
[126] D.-W. Suh, S.-J. Park, C.-S. Oh, S.-J. Kim, *Scr. Mater.* **2007**, *57*, 1097.
[127] B. C. de Cooman, *Curr. Opin. Solid State Mater. Sci.* **2004**, *8*, 285.
[128] S. Traint, A. Pichler, M. Blaimschein, B. Bohler, C. Krempaysky, E. Werner, in *Int. Conf. on Advanced High Strength Sheet Steels for Automotive Applications Proc.* (Eds: R. E. Ashburn, M. A. Baker), Association for Iron & Steel Technology, Colorado **2004**, p. 79.
[129] S. I. Kim, Y. H. Jin, J. N. Kwak, K. G. Chin, in *MS&T 2008: Proc. from the Materials Science & Technology Conf.*, MS&T Partner Societies, Pittsburgh, **2008**, p. 1794.
[130] W. Bleck, A. Frehn, J. Ohlert, in *Niobium Science & Technology: Proc. of the Int. Symp. Niobium 2001* (Ed: Minerals, Metals and Materials Society), The Minerals, Metals & Materials Society, Florida, **2001**, pp. 727.
[131] T. Heller, I. Heckelmann, T. Gerber, T. W. Schaumann, in *Proc. of Recent Advanced of Niobium Containing Materials in Europe* (Eds: K. Hulka, C. Klinkenberg, H. Mohrbacher), Verl. Stahleisen GmbH, Düsseldorf **2005**, p. 21.
[132] S. Traint, A. Pichler, R. Sierlinger, H. Pauli, E. A. Werner, *Steel Res. Int.* **2006**, *77*, 641.
[133] H. K. D. H. Bhadeshia, *ISIJ Int.* **2002**, *42*, 1059.
[134] W. Bleck, S. Papaefthymiou, A. Frehn, *Steel Res. Int.* **2004**, *75*, 704.
[135] K.-I. Sugimoto, R. Kikuchi, S.-I. Hashimoto, *Steel Res.* **2002**, *73*, 253.
[136] G. N. Haidemenopoulos, A. T. Kermanidis, C. Malliaros, H. H. Dickert, P. Kucharzyk, W. Bleck, *Mater. Sci. Eng. A* **2013**, *573*, 7.
[137] J. Chiang, J. D. Boyd, A. K. Pilkey, *Mater. Sci. Eng. A* **2015**, *638*, 132.
[138] K.-I. Sugimoto, M. Kobayashi, S.-I. Yasuki, S.-I. Hashimoto, *Mater. Trans.* **1995**, *36*, 632.
[139] K.-I. Sugimoto, M. Kobayashi, S.-I. Hashimoto, *Metall. Trans. A* **1992**, *23*, 3085.

[140] A. K. Sachdev, *Acta Metall.* **1983**, *31*, 2037.
[141] J. J. Yi, K. J. Yu, I. S. Kim, S. J. Kim, *Metall. Trans. A* **1983**, *14*, 1497.
[142] K.-I. Sugimoto, M. Mukherjee, in *Automotive Steels: Design, Metallurgy, Processing and Applications* (Eds: R. Rana, S. B. Singh), Woodhead Publishing, Cambridge **2017**, p. 217.
[143] G. Frommeyer, U. Brüx, P. Neumann, *ISIJ Int.* **2003**, *43*, 438.
[144] H. Ding, H. Ding, D. Song, Z. Tang, P. Yang, *Mater. Sci. Eng. A* **2011**, *528*, 868.
[145] A. Petein, P. J. Jacques, *Steel Res. Int.* **2004**, *75*, 724.
[146] L. A. Barrales-Mora, Y. Lu, D. A. Molodov, *Steel Res. Int.* **2011**, *82*, 119.
[147] A. Belyakov, R. Kaibyshev, V. Torganchuk, *Steel Res. Int.* **2017**, *88*, 171.
[148] F. Berrenberg, C. Haase, L. A. Barrales-Moraa, D. A. Molodov, *Mater. Sci. Eng. A* **2017**, *681*, 56.
[149] K. A. Ofei, L. Zhao, J. Sietsma, *Steel Res. Int.* **2012**, *83*, 363.
[150] W. Song, T. Ingendahl, W. Bleck, *Acta Metall. Sin. (English Lett.)* **2014**, *27*, 546.
[151] X. Sun, H. Wang, P. Yang, W. Mao, *Steel Research Int.* **2014**, *85*, 1465.
[152] A. Saeed-Akbari, A. Schwedt, W. Bleck, *Scr. Mater.* **2012**, *66*, 1024.
[153] H. Yang, J. Li, P. Yang, *Steel Res. Int.* **2015**, *86*, 576.
[154] P. Yang, T. Y. Liu, F. Y. Lu, L. Meng, *Steel Res. Int.* **2012**, *83*, 368.
[155] A. Saeed-Akbari, L. Mosecker, A. Schwedt, W. Bleck, *Metall. Mater. Trans. A* **2012**, *43*, 1688.
[156] D. Raabe, C. C. Tasan, H. Springer, M. Bausch, *Steel Res. Int.* **2015**, *86*, 1127.
[157] S. Sato, M. Ichinose, Y. Hirotsu, Y. Inoue, *ISIJ Int.* **1989**, *29*, 868.
[158] M. Koyama, T. Sawaguchi, T. Lee, C. S. Lee, K. Tsuzakia, *Mater. Sci. Eng. A* **2011**, *528*, 7310.
[159] A. Dumay, J. P. Chateau, S. Allain, S. Migot, O. Bouaziz, *Mater. Sci. Eng. A* **2008**, *483–484*, 184.
[160] Y. S. Chun, J. S. Kim, K. T. Park, Y. K. Lee, C. S. Lee, *Mater. Sci. Eng. A* **2012**, *533*, 87.
[161] D. V. Edmonds, K. He, F. C. Rizzo, B. C. De Cooman, D. K. Matlock, J. G. Speer, *Mater. Sci. Eng. A* **2006**, *438–440*, 25.
[162] J. G. Speer, E. De Moor, K. O. Findley, D. K. Matlock, B. C. De Cooman, D. V. Edmonds, *Metall. Mater. Trans. A* **2011**, *42*, 3591.
[163] L. Wang, W. Feng, in *Advanced Steels* (Eds: Y. Weng, H. Dong, Y. Gan), Springer-Verlag Berlin Heidelberg and Metallurgical Industry Press, New York City **2011**, p. 255.
[164] P. R. Spena, L. Cortese, M. De Maddis, F. Lombardi, *Steel Res. Int.* **2016**, *87*, 1592.
[165] X. Tan, Y. Xu, X. Yang, Di. Wu, *Mater. Sci. Eng. A* **2014**, *589*, 101.
[166] X. C. Xiong, B. Chen, M. X. Huang, J. F. Wang, L. Wang, *Scr. Mater.* **2013**, *68*, 321.
[167] E. De Moor, J. G. Speer, D. K. Matlock, J. H. Kwak, S. B. Lee, *Steel Res. Int.* **2012**, *83*, 322.
[168] B. C. de Cooman, J. G. Speer, *Steel Res. Int.* **2006**, *77*, 634.
[169] X. H. Hu, X. Sun, L. G. Hector, Y. Ren, *Acta Mater.* **2017**, *132*, 230.
[170] J. Shi, X. Sun, M. Wang, W. Hui, H. Dong, W. Cao, *Scr. Mater.* **2010**, *63*, 815.
[171] W. Q. Cao, C. Wang, J. Shi, M. Q. Wang, W. J. Hui, H. Dong, *Mater. Sci. Eng. A* **2011**, *528*, 6661.
[172] S. Lee, B. C. De Cooman, *Steel Res. Int.* **2015**, *86*, 1170.
[173] H. F. Xu, J. Zhao, W. Q. Cao, J. Shi, C. Y. Wang, J. Li, H. Dong, *Mater. Sci. Eng. A* **2012**, *532*, 435.
[174] D. Raabe, S. Sandlöbes, J. Millan, D. Ponge, H. Assadi, M. Herbig, P.-P. Choi, *Acta Mater.* **2013**, *61*, 6132.
[175] S.-J. Lee, S. Lee, B. C. De Cooman, *Scr. Mater.* **2011**, *64*, 649.
[176] C. Wang, S. Jie, C. Y. Wang, W. J. Hui, M. Q. Wang, H. D. Han, W. Q. Cao, *ISIJ Int.* **2011**, *51*, 651.
[177] R. Sun, W. Xu, C. Wang, J. Shi, H. Dong, W. Cao, *Steel Res. Int.* **2012**, *83*, 316.
[178] J. Han, S. J. Lee, C. Y. Lee, S. Lee, S. Y. Jo, Y. K. Lee, *Mater. Sci. Eng. A* **2015**, *633*, 9.
[179] D. W. Suh, J. H. Ryu, M. S. Joo, H. S. Yang, K. Lee, H. K. D. H. Bhadeshia, *Metall. Mater. Trans. A* **2013**, *44*, 286.
[180] M. I. Tzini, P. Sarafoglou, A. Stieben, G. Haidemenopoulos, W. Bleck, *Steel Res. Int.* **2016**, *87*, 1686.
[181] K.-I. Sugimoto, H. Tanino, J. Kobayashi, *Steel Res. Int.* **2015**, *86*, 1151.
[182] X. Zhao, Y. Shen, L Qiu, Y. Liu, X. Sun, L. Zuo, *Materials* **2014**, *7*, 7891.
[183] L. Zhang, X. Huang, Y. Guo, Y. Wang, J. Gao, G. Dai, *Steel Res. Int.* **2017**, *87*, 60.
[184] C. Wang, W. Cao, J. Shi, C. Huang, H. Dong, *Mater. Sci. Eng. A* **2013**, *562*, 89.
[185] S. Lee, B. C. De Cooman, *Metall. Mater. Trans. A* **2014**, *45*, 709.